Vibrational power flow analysis of Timoshenko microbeams with a crack

Xin-Wei Wu[a], Lin-Feng Zhu[a*], Zhang-Ming Wu[b,c], Liao-Liang Ke[a*]

[a] *School of Mechanical Engineering, Tianjin University, Tianjin, 300350, China*

[b] *School of Mechanical Engineering and Mechanics, Ningbo University, Ningbo, 315211, China*

[c] *School of Engineering, Cardiff University, Cardiff CF24 3AA, UK*

In this paper, an analytical model based on the modified couple stress theory and Timoshenko beam theory is developed to study the vibrational power flow of a microbeam with a crack. The open edge crack on the microbeam is modeled as a rotational spring, which connects the two segments of the microbeam separated by the crack location. The governing equations of the cracked microbeam are derived from Hamilton's principle. By introducing the differential operator method, the differential equations are transformed into algebraic equations, and the governing equations are decoupled. The wave propagation method is applied to solve the vibrational problem of a cracked microbeam under a transverse harmonic excitation. Both the input power flow and the transmitted power flow in the cracked microbeam are computed and analyzed. The size effect of the cracked microbeam in terms of material length scale is firstly analyzed. Subsequently, the effects of crack depth and crack location on the input and transmitted power flows are investigated. It is found that the existence of crack significantly changes the transmission characteristics of the power flow.

Keywords: Vibrational power flow; Timoshenko microbeam; Edge crack; Size effect

*Corresponding author.

E-mail address: llke@tju.edu.cn (Liao-Liang Ke); lfzhu@tju.edu.cn (Lin-Feng Zhu)

1. Introduction

With the advanced development of modern manufacturing technology, miniaturized devices, such as micro- and nano-electro-mechanical system (MEMS, NEMS) etc., has been rapidly applied in many engineering areas. Energy dissipation in micro-/nano-resonators has always been a key problem and a major handicap that restricts their performance and applications. When micro- and nano-structures are subjected to internal or external excitation forces, damages may occur in some parts of the structural elements [1-6]. Therefore, there remains ongoing interests to study the vibration energy transmission mechanism of micro-/nano- devices.

Mechanical structures subjected to internal or external loads will inevitably produce a certain degree of structure-borne noise, which may induce damages to the structures. To analyze such structure-borne noise and structural damage, it is necessary to evaluate the vibration intensity for each part of the structure. The vibrational power flow not only includes amplitudes of velocity and force but also establishes a relationship between them. It thus provides a new perspective and powerful tool for researchers to study the vibration energy transfer mechanism. Up to now, a large number of research works had been focused on the analysis of vibration power flow of macrostructures. However, to the best of authors' knowledge, no work had been reported on the vibration power flow analysis of micro-/nano-structures. Liu et al. [7] studied the vibrational power flow in a cylindrical shell filled with fluid under a dynamic force loading. Cho et al. [8] developed the structural intensity technique to analyze the vibrational energy flow in plates that are under a harmonic excitation. Liu and Niu [9] established an energy flow model for functionally graded Euler-Bernoulli beams. Sheng et al. [10] analyzed the effect of the distributive mass of spring on the vibrational power flow from experimental tests. Zheng et al. [11] predicted the energy contribution of the interior vibrational noise in a high-speed train using finite element method. Wang and Chen [12] studied the energy intensity of plates subjected to thermal load. Ma et al. [13] applied the structural intensity method to analyze the energy flow transmission behaviors in aero-engine casing structures. Li et al. [14] performed the vibrational power flow analysis of the circular plate with a surface crack using the structure-borne sound method. Zhu et al. [15] investigated the wave and power flow in a cylindrical shell with a surface circumferential crack. Xu et al. [16] adopted the vibrational power flow to study nonlinear dynamic behaviors of the rotating blade with a breathing crack. Zhu et al. [17] analyzed the vibrational power flow of cracked functionally graded beams and highlighted the influence of crack location, crack depth and gradient index to the power flow. Zheng et al. [18]

analyzed the dynamic response of the cracked fluid-filled cylindrical shell and presented a damage detection method based on the energy flow.

Although no research works had been reported for the power flow analysis of microscale and nanoscale structures, there have been many works that were performed on the vibration and wave propagation analysis of microscale and nanoscale structures. The vibrations of micro-/nano- beams [20-26], plates [27-31] and shells [32-34] have being analyzed by using nonlocal theories. Based on the modified couple stress theory [19], Ma et al. [20] developed a model for Timoshenko microbeams and analyzed the size effects on the vibration response, furthermore, the size effect on vibration of the functionally graded microbeams [21], composite microbeams [22], and multiple-layer microbeams [23] were analyzed by various non-calssical theories. Giannakopoulos and Stamoulis [24] analyzed the size effects of beam bending and cracked bar tension by the gradient elasticity theory. Zhao et al. [25] proposed the analytical solution of coupled thermoelastic forced vibration of nonlocal beams utilizing Green's functions. Kumar and Kumar [26] analyzed the effect of temperature parameters on thermoelastic vibration in micro-/nano-beam resonators. The free vibration analysis of Mindlin nanoplates [27], functionally graded micro-/nano-plates [28], graded porous microplates [29], and three-layered microplates [30, 31] were analyzed in detail. Zhou and Wang [32] analyzed the vibration behaviour of a cylindrical microshell filled with fluid based on the modified couple stress theory. Gholami et al. [33] developed a size-dependent shear deformable shell model based on the strain gradient elasticity theory and analyzed the size-dependent buckling and vibration of micro-/nano-shells. Ghasemi and Mohandes [34] analyzed the frequencies of fiber-metal laminated cylindrical micro-/nano-shells.

All the reports listed above are for intact structures, and vibration analysis of cracked structures has also been reported [35-39]. The vibration models of microbeams with crack by modified couple stress theory were established and studied in references [35, 36]. Zhou et al. [37] studied the characteristics of vibrations of electrostatically actuated microbeams with slant crack. Akbas [38] investigated the vibration of a cracked functionally graded microbeam with damping effect. Ziaee [39] analyzed the thermal effect on the vibration of micro-/nano-plates with a cut-out by the Ritz method. Wave propagation and reflection is a hot topic in the analysis of energy transfer in micro-/nano-structures. Most recently, Bahrami and his co-authors studied the wave propagation and reflection in intact nanobeams and nanoplates [40, 41, 42], cracked nanobeams [43] and nanorods [44]. Ilkhani et al. [45] considered wave propagation in rectangular thin nanoplates. Ebrahimi et al. [46] studied energy reflection and transmission in thermoelastic nanoplates using a novel nonlocal strain

gradient theory. Zeighampour et al. [47] presented wave propagation in fluid-conveying nanotubes by using the nonlocal strain gradient theory. The introduction of the concept of power flow will overcome the shortcoming that energy alone cannot reflect the vibration intensity of each part of the structure. The influence of size effects on power flow will be presented for the first time in this paper.

In this paper, vibrational power flow in a cracked microbeam is studied based on the Timoshenko beam theory and modified couple stress theory. The open edge crack is modelled as a rotational spring. The Hamilton's principle is employed to derive the governing equations, which are six-order coupled partial differential equations. By introducing the differential operator, the governing equations are decoupled, and the analytical solution are obtained. The wave propagation method is applied to analyze the vibrational response of the cracked microbeam under a harmonic excitation. Both the input and transmitted power flows are derived and analyzed. The influences of the scale parameter, crack location and crack depth on the input and transmitted power flows are investigated in detail.

2. The modified couple stress theory

In 2002, Yang and his co-authors first proposed the modified couple stress theory, from which we have the following equations [19]

$$\varepsilon_{ij} = \frac{1}{2}\left(u_{i,j} + u_{j,i}\right), \tag{1}$$

$$\chi_{ij} = \frac{1}{2}\left(\theta_{i,j} + \theta_{j,i}\right), \tag{2}$$

$$\theta_i = \frac{1}{2} e_{ijk} u_{k,j}, \tag{3}$$

$$\sigma_{ij} = \lambda \varepsilon_{kk} \delta_{ij} + 2\mu \varepsilon_{ij}, \tag{4}$$

$$m_{ij} = 2\mu l^2 \chi_{ij}, \tag{5}$$

where σ and ε are Cauchy stress tensor and strain tensor, respectively; u and θ are displacement and rotation angle, respectively; χ is the symmetric curvature tensor; m is the deviatoric part of the couple stress tensor; λ and μ are Lame's constants; l is material length scale parameter.

3. The cracked beam model

A cracked microbeam subjected to an excitation force $F=F_0\ e^{i\Omega t}$ is shown in Fig. 1 where Ω is the vibrational frequency. The open edge crack with depth a is located away L from the location of the excitation

force. The thickness and width of the microbeam are h and b, respectively. External excitation is applied at the origin of the coordinate system. The coordinate system (x, z) is established with respect to that z-axis is oriented vertically downward, and x-axis is along the mid-plane of the microbeam.

As shown in Fig. 2, the crack position is modeled as a rotational spring. For beam structures with transverse bending vibration, the bending moment dominates the vibrational behavior, therefore the bending stiffness at the crack section can be approximated by the stiffness of the rotating spring [17]. The premises of this spring modelling approach are that the crack does not propagate, always remains open and is perpendicular to the upper surface of the beam. Taking the crack as a dividing point, the beam is separated into two segments, which are connected by a rotating spring. The bending stiffness S_T of the spring is defined as

$$S_T = \frac{1}{W}, \tag{6}$$

where W is the flexibility. The differential relationship between the crack depth a and the flexibility W is given by

$$\frac{\left(1-\upsilon^2\right)K_1^2}{E} = \frac{M^2}{2}\frac{\mathrm{d}W}{\mathrm{d}a}. \tag{7}$$

In Eq. (7), M is the bending moment at the cracked section; K_1 denotes the stress intensity factor subjected to the bending load. In the present analysis, we employ the stress intensity factors (SIFs) of the cracked macroscale beam to approximately evaluate the SIFs of the cracked microbeam. Therefore, the relation between SIFs and crack depth is expressed as [17]

$$K_1 = \frac{6M\sqrt{\pi h\varsigma}}{h^2} f(\varsigma),\ \varsigma = \frac{a}{h}, \tag{8}$$

where

$$f\left(\varsigma\right) = 1.150 - 1.662\varsigma + 21.667\varsigma^2 - 192.451\varsigma^3 + 909.375\varsigma^4$$
$$-2124.310\varsigma^5 + 2395.830\varsigma^6 - 1031.750\varsigma^7.$$

Then, the flexibility W is obtained from Eqs. (7)-(8)

$$W = \frac{72\pi\left(1-\mu^2\right)}{Eh^2}\int_0^{\varsigma} \varsigma f^2\left(\varsigma\right)\mathrm{d}\varsigma. \tag{9}$$

4. Timoshenko beam model

In the Timoshenko beam theory, the displacement of an arbitrary point in the beam along the *x*- and *z*-axes, represented as $\bar{u}$ and $\bar{w}$ respectively, are expressed as

$$\bar{u}(x,z,t)=z\psi(x,t),\quad \bar{w}(x,z,t)=w(x,t), \tag{10}$$

where $w(x, t)$ is the displacement component in the mid-plane; $\psi(x, t)$ is the rotation of beam cross-section; t is time. The linear strain-displacement relation is defined as

$$\varepsilon_{xx}=z\frac{\partial\psi}{\partial x},\ \varepsilon_{xz}=\frac{1}{2}\left(\psi+\frac{\partial w}{\partial x}\right),\ \varepsilon_{yy}=\varepsilon_{zz}=\varepsilon_{xy}=\varepsilon_{yz}=0. \tag{11}$$

From Eq. (4), the normal stress σ_{xx} and shear stress σ_{xz} are given by

$$\sigma_{xx}=\frac{E}{1-\upsilon^2}\varepsilon_{xx},\ \sigma_{xz}=\frac{E}{2(1+\upsilon)}\varepsilon_{xz}, \tag{12}$$

where E is Young's modulus, υ is Poisson's ratio. Substituting Eq. (10) into Eq. (3) gives

$$\theta_y=\frac{1}{2}\left(\psi-\frac{\partial w}{\partial x}\right),\ \theta_x=\theta_z=0. \tag{13}$$

Applying Eqs. (2) and (13) leads to

$$\chi_{xy}=\frac{1}{4}\left(\frac{\partial\psi}{\partial x}-\frac{\partial^2 w}{\partial x^2}\right),\ \chi_{xx}=\chi_{yy}=\chi_{zz}=\chi_{xz}=\chi_{yz}=0. \tag{14}$$

Considering the locations of the external excitation force and crack, the microbeam can be separated into three segments along the axial direction, which are $(-\infty,0]$, $[0,L]$, $[L,+\infty)$, respectively.

The strain energy Π_S of the cracked Timoshenko microbeam over the entire domain Λ of the infinite long beam is expressed as

$$\begin{aligned}\Pi_S=&\frac{1}{2}\int_{-\infty}^{0}\int_A\left(\sigma_{xx}\varepsilon_{xx}+2\sigma_{xz}\varepsilon_{xz}+2m_{xy}\chi_{xy}\right)\mathrm{d}A\mathrm{d}x+\frac{1}{2}\int_0^L\int_A\left(\sigma_{xx}\varepsilon_{xx}+2\sigma_{xz}\varepsilon_{xz}+2m_{xy}\chi_{xy}\right)\mathrm{d}A\mathrm{d}x\\&+\frac{1}{2}\int_L^{+\infty}\int_A\left(\sigma_{xx}\varepsilon_{xx}+2\sigma_{xz}\varepsilon_{xz}+2m_{xy}\chi_{xy}\right)\mathrm{d}A\mathrm{d}x+\frac{1}{2}S_T\left[\delta\psi(L)\right]^2,\end{aligned} \tag{15}$$

where A is the cross-section area of the beam. The first and last terms in Eq. (15) are improper integral, and the third term denotes the elastic potential energy of a rotational spring. Herein, $\delta\psi(L)$ denotes the angle variational between the two sides of the section at the crack.

From the energy point of view, the wave propagation will eventually dissipate the strain energy of the beam. Therefore, $\lim_{x\to\pm\infty}\int_A\left(\sigma_{xx}\varepsilon_{xx}+2\sigma_{xz}\varepsilon_{xz}+2m_{xy}\chi_{xy}\right)\mathrm{d}A=0$, which indicates that the improper integrals in Eq.

(15) are integrable. Substituting Eqs. (11) and (14) into Eq. (15) gives

$$\begin{aligned}\Pi_S = &\frac{1}{2}\int_{-\infty}^{0}\left[M_{y1}\frac{\partial\psi_1}{\partial x}+Q_{z1}\left(\psi_1+\frac{\partial w_1}{\partial x}\right)+\frac{1}{2}Y_{xy1}\left(\frac{\partial\psi_1}{\partial x}-\frac{\partial^2 w_1}{\partial x^2}\right)\right]\mathrm{d}x\\ &+\frac{1}{2}\int_{0}^{L}\left[M_{y2}\frac{\partial\psi_2}{\partial x}+Q_{z2}\left(\psi_2+\frac{\partial w_2}{\partial x}\right)+\frac{1}{2}Y_{xy2}\left(\frac{\partial\psi_2}{\partial x}-\frac{\partial^2 w_2}{\partial x^2}\right)\right]\mathrm{d}x+\frac{1}{2}S_T\left[\delta\psi(L)\right]^2\\ &+\frac{1}{2}\int_{L}^{\infty}\left[M_{y3}\frac{\partial\psi_3}{\partial x}+Q_{z3}\left(\psi_3+\frac{\partial w_3}{\partial x}\right)+\frac{1}{2}Y_{xy3}\left(\frac{\partial\psi_3}{\partial x}-\frac{\partial^2 w_3}{\partial x^2}\right)\right]\mathrm{d}x,\end{aligned} \tag{16}$$

where A represents the area of the beam cross-section. The subscripts "1", "2" and "3" in M_{y1}, M_{y2}, M_{y3}, Q_{z1}, Q_{z2}, Q_{z3} and Y_{xy1}, Y_{xy2}, Y_{xy3} are used to denote the variable for each section. In general, the bending moment M_y, transverse shear force Q_z and couple moment Y_{xy} are given by

$$M_y = \int_A \sigma_x z\mathrm{d}A = D_{11}\frac{\partial\psi}{\partial x}, \tag{17}$$

$$Q_z = \int_A \sigma_{xz}\mathrm{d}A = k_s A_{55}\left(\psi+\frac{\partial w}{\partial x}\right), \tag{18}$$

$$Y_{xy} = \int_A m_{xy}\mathrm{d}A = \frac{1}{2}l^2 A_{55}\left(\frac{\partial\psi}{\partial x}-\frac{\partial^2 w}{\partial x^2}\right), \tag{19}$$

where $k_s = 5/6$ represents the shear correction factor. A_{11}, D_{11} and A_{55} are given by

$$\left\{A_{11}, D_{11}\right\} = \left\{\frac{Ebh}{1-\upsilon^2}, \frac{Ebh^3}{12\left(1-\upsilon^2\right)}\right\},\ A_{55} = \frac{Ebh}{2\left(1+\upsilon\right)}. \tag{20}$$

The kinetic energy Π_T is given by

$$\begin{aligned}\Pi_T = &\frac{1}{2}\int_{-\infty}^{0}\left[I_3\left(\frac{\partial\psi_1}{\partial t}\right)^2+I_1\left(\frac{\partial w_1}{\partial t}\right)^2\right]\mathrm{d}x+\frac{1}{2}\int_{0}^{L}\left[I_3\left(\frac{\partial\psi_2}{\partial t}\right)^2+I_1\left(\frac{\partial w_2}{\partial t}\right)^2\right]\mathrm{d}x\\ &+\frac{1}{2}\int_{L}^{+\infty}\left[I_3\left(\frac{\partial\psi_3}{\partial t}\right)^2+I_1\left(\frac{\partial w_3}{\partial t}\right)^2\right]\mathrm{d}x,\end{aligned} \tag{21}$$

where

$$\left\{I_1, I_3\right\} = \int_A \rho\left\{1, z^2\right\}\mathrm{d}A = \left\{\rho bh, \frac{\rho bh^3}{12}\right\}.$$

The work done by the force $F = F_0\,\mathrm{e}^{\mathrm{i}\Omega t}$ is written by Π_P

$$\Pi_P = \frac{1}{2}\int_{-\infty}^{\infty} F_0\mathrm{e}^{\mathrm{i}\Omega t}\delta(x)w\mathrm{d}x. \tag{22}$$

Applying the Hamilton's principle

$$\int_0^t (\delta\Pi_S + \delta\Pi_P - \delta\Pi_T)\mathrm{d}t = 0, \tag{23}$$

and substituting Eqs. (16), (21) and (22) into Eq. (23) yields

$$\begin{aligned}
0 &= \int_0^t \int_{-\infty}^0 \Lambda_1 \,\mathrm{d}x\mathrm{d}t + \int_0^t \int_0^L \Lambda_2 \,\mathrm{d}x\mathrm{d}t + \int_0^t \int_L^{+\infty} \Lambda_3 \,\mathrm{d}x\mathrm{d}t + \int_0^t F_0 \mathrm{e}^{\mathrm{i}\Omega t}\delta w_1 \mathrm{d}t + \int_0^t S_T \delta\psi(L)\delta\delta\psi(L)\mathrm{d}t \\
&= \int_0^t \int_{-\infty}^0 \Phi_1 \,\mathrm{d}x\mathrm{d}t + \int_0^t \int_0^L \Phi_2 \,\mathrm{d}x\mathrm{d}t + \int_0^t \int_L^{+\infty} \Phi_3 \,\mathrm{d}x\mathrm{d}t + \int_0^t F_0 \mathrm{e}^{\mathrm{i}\Omega t}\delta w_1 \mathrm{d}t \\
&+ \int_0^t \left\{ \left(Q_{z1} + \frac{1}{2}\frac{\partial Y_{xy1}}{\partial x} \right)\delta w_1 \Big|_{-\infty}^0 + \left(Q_{z2} + \frac{1}{2}\frac{\partial Y_{xy2}}{\partial x} \right)\delta w_2 \Big|_0^L + \left(Q_{z3} + \frac{1}{2}\frac{\partial Y_{xy3}}{\partial x} \right)\delta w_3 \Big|_L^{+\infty} \right\} \mathrm{d}t \\
&+ \int_0^t \left\{ \left(M_{y1} + \frac{1}{2}Y_{xy1} \right)\delta\psi_1 \Big|_{-\infty}^0 + \left(M_{y2} + \frac{1}{2}Y_{xy2} \right)\delta\psi_2 \Big|_0^L + \left(M_{y3} + \frac{1}{2}Y_{xy3} \right)\delta\psi_3 \Big|_L^{+\infty} \right\} \mathrm{d}t \\
&- \frac{1}{2}\int_0^t \left\{ Y_{xy1}\left(\frac{\partial\delta w_1}{\partial x} \right)\Big|_{-\infty}^0 + Y_{xy2}\left(\frac{\partial\delta w_2}{\partial x} \right)\Big|_0^L + Y_{xy3}\left(\frac{\partial\delta w_3}{\partial x} \right)\Big|_L^{+\infty} - 2S_T\delta\psi(L)\delta\left[\psi_2(L) - \psi_3(L)\right] \right\} \mathrm{d}t,
\end{aligned} \tag{24}$$

where

$$\Lambda_i = I_3 \frac{\partial\psi_i}{\partial t}\frac{\partial\delta\psi_i}{\partial t} + I_1 \frac{\partial w_i}{\partial t}\frac{\partial\delta w_i}{\partial t} - M_{yi}\frac{\partial\delta\psi_i}{\partial x} + Q_{zi}\left(\delta\psi_i + \frac{\partial\delta w_i}{\partial x} \right) + \frac{1}{2}Y_{xyi}\left(\frac{\partial\delta\psi_i}{\partial x} - \frac{\partial^2\delta w_i}{\partial x^2} \right),$$

$$\Phi_i = \left(I_3 \frac{\partial^2\psi_i}{\partial t^2} - \frac{\partial M_{yi}}{\partial x} + Q_{zi} - \frac{1}{2}\frac{\partial Y_{xyi}}{\partial x} \right)\delta\psi_i + \left(I_1 \frac{\partial^2 w_i}{\partial t^2} - \frac{\partial Q_{zi}}{\partial x} - \frac{1}{2}\frac{\partial^2 Y_{xyi}}{\partial x^2} \right)\delta w_i, (i = 1, 2, 3).$$

Setting the coefficients of $\delta\psi_i$ and δw_i (i = 1, 2, 3) to zero, the governing equations of the three sub-beams are expressed as

$$\frac{\partial Q_{zi}}{\partial x} + \frac{1}{2}\frac{\partial^2 Y_{xyi}}{\partial x^2} = I_1 \frac{\partial^2 w_i}{\partial t^2}, \tag{25}$$

$$\frac{\partial M_{yi}}{\partial x} - Q_{zi} + \frac{1}{2}\frac{\partial Y_{xyi}}{\partial x} = I_3 \frac{\partial^2\psi_i}{\partial t^2}. \tag{26}$$

The continuous conditions at the location of the excitation force x = 0 are

$$w_1 = w_2, Q_{z1} + \frac{1}{2}\frac{\partial Y_{xy1}}{\partial x} + F_0 \mathrm{e}^{\mathrm{i}\Omega t} = Q_{z2} + \frac{1}{2}\frac{\partial Y_{xy2}}{\partial x}, \tag{27a}$$

$$\psi_1 = \psi_2, M_{y1} + \frac{1}{2}Y_{xy1} = M_{y2} + \frac{1}{2}Y_{xy2}, \tag{27b}$$

$$\frac{\partial w_1}{\partial x}=\frac{\partial w_2}{\partial x}, Y_{xy1}=Y_{xy2}. \tag{27c}$$

The continuous conditions at the crack location $x = L$ are

$$Q_{z2}+\frac{1}{2}\frac{\partial Y_{xy2}}{\partial x}=Q_{z3}+\frac{1}{2}\frac{\partial Y_{xy3}}{\partial x}, w_2=w_3,\ M_{y2}=M_{y3}, \tag{28a}$$

$$S_T\left(\psi_3-\psi_2\right)=M_{y3}+\frac{1}{2}Y_{xy3}, Y_{xy2}=Y_{xy3},\ \frac{\partial w_2}{\partial x}=\frac{\partial w_3}{\partial x}. \tag{28b}$$

Substituting Eqs. (17)-(19) into Eqs. (25) and (26) yields

$$k_s A_{55}\left(\frac{\partial \psi_i}{\partial x}+\frac{\partial^2 w_i}{\partial x^2}\right)+\frac{l^2 A_{55}}{4}\left(\frac{\partial^3 \psi_i}{\partial x^3}-\frac{\partial^4 w_i}{\partial x^4}\right)=I_1\frac{\partial^2 w_i}{\partial t^2}, \tag{29}$$

$$D_{11}\frac{\partial^2 \psi_i}{\partial x^2}-k_s A_{55}\left(\psi_i+\frac{\partial w_i}{\partial x}\right)+\frac{l^2 A_{55}}{4}\left(\frac{\partial^2 \psi_i}{\partial x^2}-\frac{\partial^3 w_i}{\partial x^3}\right)=I_3\frac{\partial^2 \psi_i}{\partial t^2}. \tag{30}$$

Introducing the dimensionless quantities

$$\zeta=\frac{x}{h},\ \tilde{w}=\frac{w}{h},\ \left(\bar{I}_1,\bar{I}_3\right)=\left(1,\frac{I_3}{I_1h^2}\right),\ \tilde{\psi}=\psi,\ l_0=\frac{l}{h}, \tag{31a}$$

$$\left(a_{55},d_{11}\right)=\left(\frac{A_{55}}{A_{11}},\frac{D_{11}}{A_{11}h^2}\right),\ \tau=\frac{t}{h}\sqrt{\frac{A_{11}}{I_1}},\ \omega=\Omega h\sqrt{\frac{I_1}{A_{11}}}, \tag{31b}$$

Eqs. (29) and (30) are expressed in dimensionless forms as

$$k_s a_{55}\left(\frac{\partial^2 \tilde{w}_i}{\partial \zeta^2}+\frac{\partial \tilde{\psi}_i}{\partial \zeta}\right)+\frac{l_0^2 a_{55}}{4}\left(\frac{\partial^3 \tilde{\psi}_i}{\partial \zeta^3}-\frac{\partial^4 \tilde{w}_i}{\partial \zeta^4}\right)=\bar{I}_1\frac{\partial^2 \tilde{w}_i}{\partial \tau^2}, \tag{32}$$

$$d_{11}\frac{\partial^2 \tilde{\psi}_i}{\partial \zeta^2}-k_s a_{55}\left(\tilde{\psi}_i+\frac{\partial \tilde{w}_i}{\partial \zeta}\right)+\frac{l_0^2 a_{55}}{4}\left(\frac{\partial^2 \tilde{\psi}_i}{\partial \zeta^2}-\frac{\partial^3 \tilde{w}_i}{\partial \zeta^3}\right)=\bar{I}_3\frac{\partial^2 \tilde{\psi}_i}{\partial \tau^2}. \tag{33}$$

According to the wave propagation theory [42], the displacement and rotation of the microbeam under a harmonic excitation are expressed as

$$\tilde{\psi}_i(\zeta,\tau)=\Psi_i(\zeta)\mathrm{e}^{\mathrm{i}\omega\tau},\ \tilde{w}_i(\zeta,\tau)=W_i(\zeta)\mathrm{e}^{\mathrm{i}\omega\tau}. \tag{34}$$

With the method of variable separation, the following amplitude equations are obtained by substituting Eq. (34) into Eqs. (32) and (33)

$$k_s a_{55}\left(D^2W_i+D\Psi_i\right)+\frac{a_{55}l_0^2}{4}\left(D^3\Psi_i-D^4W_i\right)=-\omega^2\bar{I}_1W_i, \tag{35}$$

$$d_{11}D^2\Psi_i - k_s a_{55}\left(DW_i + \Psi_i\right) + \frac{a_{55}l_0^2}{4}\left(D^2\Psi_i - D^3W_i\right) = -\omega^2\bar{I}_3\Psi_i, \tag{36}$$

where the differential operator $D = \mathrm{d} / \mathrm{d}\zeta$. The introduction of differential operator transforms the differential equation into "algebraic equation", Eq. (35) can be further rewritten as

$$\left(k_s a_{55}D^2 - \frac{a_{55}l_0^2}{4}D^4 + \omega^2\bar{I}_1\right)W_i + \left(k_s a_{55}D + \frac{a_{55}l_0^2}{4}D^3\right)\Psi_i = 0. \tag{37}$$

Substituting Eq. (37) into Eq. (36), we have

$$\begin{aligned}&\frac{a_{55}d_{11}l_0^2}{4}D^6W_i + \left(\frac{a_{55}l_0^2\omega^2\bar{I}_3}{4} - k_s a_{55}^2 l_0^2 - a_{55}k_s d_{11}\right)D^4W_i \\ &-\left(k_s a_{55}\bar{I}_3\omega^2 + \frac{a_{55}l_0^2\bar{I}_1\omega^2}{4} + \bar{I}_1\omega^2 d_{11}\right)D^2W_i - \left(\bar{I}_1\bar{I}_3\omega^4 - k_s\bar{I}_1 a_{55}\omega^2\right)W_i = 0,\end{aligned} \tag{38}$$

$$\begin{aligned}&\frac{a_{55}d_{11}l_0^2}{4}D^6\Psi_i + \left(\frac{a_{55}l_0^2\omega^2\bar{I}_3}{4} - k_s a_{55}^2 l_0^2 - a_{55}k_s d_{11}\right)D^4\Psi_i \\ &-\left(k_s a_{55}\bar{I}_3\omega^2 + \frac{a_{55}l_0^2\bar{I}_1\omega^2}{4} + \bar{I}_1\omega^2 d_{11}\right)D^2\Psi_i - \left(\bar{I}_1\bar{I}_3\omega^4 - k_s\bar{I}_1 a_{55}\omega^2\right)\Psi_i = 0.\end{aligned} \tag{39}$$

By introducing differential operators, the complex high-order differential equations are decoupled, which makes it very convenient to obtain their analytical solutions. This method was also originally applied by Lekhnitskii to obtain analytical solutions for anisotropic plates [48]. The characteristic equation of the ordinary differential equations (38) and (39) is

$$a_1\lambda^6 + a_2\lambda^4 + a_3\lambda^2 + a_4 = 0, \tag{40}$$

where

$$a_1 = \frac{a_{55}d_{11}l_0^2}{4}, a_2 = \frac{a_{55}l_0^2\omega^2\bar{I}_3}{4} - k_s a_{55}^2 l_0^2 - a_{55}k_s d_{11},$$

$$a_3 = -k_s a_{55}\bar{I}_3\omega^2 - \frac{a_{55}l_0^2\bar{I}_1\omega^2}{4} - \bar{I}_1\omega^2 d_{11}, a_4 = -\bar{I}_1\bar{I}_3\omega^4 + k_s\bar{I}_1 a_{55}\omega^2.$$

The general solutions for Eqs. (35) and (36) are assumed as

$$W_i = f_{1i}\mathrm{e}^{k_1\zeta} + f_{2i}\mathrm{e}^{-k_1\zeta} + f_{3i}\mathrm{e}^{k_2\zeta} + f_{4i}\mathrm{e}^{-k_2\zeta} + f_{5i}\mathrm{e}^{k_3\zeta} + f_{6i}\mathrm{e}^{-k_3\zeta}, \tag{41}$$

$$\Psi_i = q_1 f_{1i}\mathrm{e}^{k_1\zeta} - q_1 f_{2i}\mathrm{e}^{-k_1\zeta} + q_2 f_{3i}\mathrm{e}^{k_2\zeta} - q_2 f_{4i}\mathrm{e}^{-k_2\zeta} + q_3 f_{5i}\mathrm{e}^{k_3\zeta} - q_3 f_{6i}\mathrm{e}^{-k_3\zeta}, \tag{42}$$

where

$$k_1=\sqrt{Y_1^{\frac{1}{3}}+Y_2^{\frac{1}{3}}-\frac{a_2}{3a_1}},\ k_2=\sqrt{\alpha Y_1^{\frac{1}{3}}+\alpha^2 Y_2^{\frac{1}{3}}-\frac{a_2}{3a_1}},\ k_3=\sqrt{\alpha^2 Y_1^{\frac{1}{3}}+\alpha Y_2^{\frac{1}{3}}-\frac{a_2}{3a_1}}, \tag{43}$$

$$\begin{pmatrix}Y_1\\Y_2\end{pmatrix}=\frac{9a_1a_2a_3-27a_1^2a_4-2a_2^3}{54a_1^3}\pm\left[\left(\frac{9a_1a_2a_3-27a_1^2a_4-2a_2^3}{54a_1^3}\right)^2+\left(\frac{3a_1a_3-a_2^2}{9a_1^2}\right)^3\right]^{\frac{1}{2}}, \tag{44}$$

$$\alpha=\frac{-1+\sqrt{3}\mathrm{i}}{2}. \tag{45}$$

Substituting Eqs. (41) and (42) into Eq. (35), we can get

$$q_i=\frac{a_{55}l_0^2k_i^4-4k_sa_{55}k_i^2-4\omega^2\bar{I}_i}{a_{55}l_0^2k_i^3+4k_sa_{55}k_i},\ i=1,2,3. \tag{46}$$

5. The intact microbeam

As shown in Fig. 3(a), an infinite intact microbeam subjected to a transverse harmonic excitation $F_0\,\mathrm{e}^{\mathrm{i}\Omega t}$ is firstly studied. There are two kinds of waves diffused away from the excitation force. The intact microbeam is separated into two segments at the location of the driving source. The rotation and transverse responses of each segment are expressed in the following dimensionless form

$$\begin{pmatrix}W_1\\\Psi_1\end{pmatrix}=\begin{pmatrix}f_{11} & f_{31} & f_{51}\\ q_1f_{11} & q_2f_{31} & q_3f_{51}\end{pmatrix}\begin{pmatrix}\mathrm{e}^{k_1\zeta}\\ \mathrm{e}^{k_2\zeta}\\ \mathrm{e}^{k_3\zeta}\end{pmatrix}, \tag{47}$$

for $\zeta\leq 0$ and

$$\begin{pmatrix}W_2\\\Psi_2\end{pmatrix}=\begin{pmatrix}f_{22} & f_{42} & f_{62}\\ -q_1f_{22} & -q_2f_{42} & -q_3f_{62}\end{pmatrix}\begin{pmatrix}\mathrm{e}^{-k_1\zeta}\\ \mathrm{e}^{-k_2\zeta}\\ \mathrm{e}^{-k_3\zeta}\end{pmatrix}, \tag{48}$$

for $\zeta > 0$.

The subscripts "1" and "2" in W_1, W_2 and Ψ_1, Ψ_2 are used to distinguish between sections. When the wavenumber k_i (i= 1, 2, 3) is a real number, the vibration of the microbeam is a decaying motion, while if the wavenumber is a pure imaginary number, it indicates that the microbeam is a propagating motion with the constant amplitude. The continuity conditions for intact microbeam at the point $\zeta = 0$ can be given as

$$W_1=W_2,\Psi_1=\Psi_2,\frac{\partial W_1}{\partial\zeta}=\frac{\partial W_2}{\partial\zeta}, \tag{49a}$$

$$k_s a_{55}\left(\Psi_1+\frac{\partial W_1}{\partial\zeta}\right)+\frac{l_0^2 a_{55}}{4}\left(\frac{\partial^2\Psi_1}{\partial\zeta^2}-\frac{\partial^3 W_1}{\partial\zeta^3}\right)+\frac{F_0}{A_{11}}= k_s a_{55}\left(\Psi_2+\frac{\partial W_2}{\partial\zeta}\right)+\frac{l_0^2 a_{55}}{4}\left(\frac{\partial^2\Psi_2}{\partial\zeta^2}-\frac{\partial^3 W_2}{\partial\zeta^3}\right), \tag{49b}$$

$$d_{11}\Psi_1+\frac{l_0^2 a_{55}}{4}\left(\frac{\partial\Psi_1}{\partial\zeta}-\frac{\partial^2 W_1}{\partial\zeta^2}\right)=d_{11}\Psi_2+\frac{l_0^2 a_{55}}{4}\left(\frac{\partial\Psi_2}{\partial\zeta}-\frac{\partial^2 W_2}{\partial\zeta^2}\right), \tag{49c}$$

$$\frac{l_0^2 a_{55}}{2}\left(\frac{\partial\Psi_1}{\partial\zeta}-\frac{\partial^2 W_1}{\partial\zeta^2}\right)=\frac{l_0^2 a_{55}}{2}\left(\frac{\partial\Psi_2}{\partial\zeta}-\frac{\partial^2 W_2}{\partial\zeta^2}\right). \tag{49d}$$

Substituting Eqs. (47) and (48) into Eqs. (49), we have

$$\mathbf{Cf}=\mathbf{Q}, \tag{50}$$

where

$$\mathbf{f}=\left(f_{11}, f_{22}, f_{31}, f_{42}, f_{51}, f_{62}\right)^{\mathrm{T}},$$

$$\mathbf{Q}=\left(0,0,0,F_0/A_{11},0,0\right)^{\mathrm{T}},$$

$$\mathbf{C}=\begin{bmatrix} 1 & -1 & 1 & -1 & 1 & -1 \\ q_1 & q_1 & q_2 & q_2 & q_3 & q_3 \\ k_1 & k_1 & k_2 & k_2 & k_3 & k_3 \\ \gamma_{11} & \gamma_{11} & \gamma_{21} & \gamma_{21} & \gamma_{31} & \gamma_{31} \\ \gamma_{12} & -\gamma_{12} & \gamma_{22} & -\gamma_{22} & \gamma_{32} & -\gamma_{32} \\ \gamma_{13} & -\gamma_{13} & \gamma_{23} & -\gamma_{23} & \gamma_{33} & -\gamma_{33} \end{bmatrix},$$

with

$$\gamma_{i1}=k_s a_{55}\left(k_i+q_i\right)+\frac{l_0^2 a_{55}}{4}\left(k_i^2 q_i-k_i^3\right),\ \gamma_{i2}=d_{11}k_i q_i+\frac{l_0^2 a_{55}}{4}\left(k_i q_i-k_i^2\right),\ \gamma_{i3}=k_i q_i-k_i^2,\left(i=1,2,3\right).$$

Then, the unknown coefficients f_{11}, f_{22}, f_{31}, f_{42}, f_{51}, f_{62} can be obtained by solving Eq. (50).

6. The cracked microbeam

The forced waves and reflected waves around crack location in the cracked microbeam that is driven by the external force are illustrated in Fig. 3(b). The crack changes the propagation path of traveling waves, some of which are reflected when they arrive the crack. The cracked beam is divided into three segments with respect to locations of the crack and excitation position. The characteristics of wave propagation in each section are different. Segment "1" only contains the wave propagating to the left from the location of excitation; segment

"2" contains both the wave propagating to the right from the location of excitation and part of the wave reflected by the crack; and segment "3" only contains part of the wave propagating to the right through the crack.

For each segment, the vibration response of the microbeam is assumed in a dimensionless form as

$$\begin{pmatrix} W_i \\ \Psi_i \end{pmatrix} = \begin{pmatrix} f_{1i} & f_{2i} & f_{3i} & f_{4i} & f_{5i} & f_{6i} \\ q_1 f_{1i} & -q_1 f_{2i} & q_2 f_{3i} & -q_2 f_{4i} & q_3 f_{5i} & -q_3 f_{6i} \end{pmatrix} \{\eta\}, \tag{51}$$

where

$$\{\eta\} = \left\{ e^{k_1\zeta}, e^{-k_1\zeta}, e^{k_2\zeta}, e^{-k_2\zeta}, e^{k_3\zeta}, e^{-k_3\zeta} \right\}^{\mathrm{T}}, \ i = 1, 2, 3. \tag{52}$$

The dimensionless forms of the continuous conditions at the crack location ($\zeta = L / h = L_1$) are

$$k_s a_{55} \left(\Psi_2 + \frac{\partial W_2}{\partial \zeta} \right) + \frac{l_0^2 a_{55}}{4} \left(\frac{\partial^2 \Psi_2}{\partial \zeta^2} - \frac{\partial^3 W_2}{\partial \zeta^3} \right) = k_s a_{55} \left(\Psi_3 + \frac{\partial W_3}{\partial \zeta} \right) + \frac{l_0^2 a_{55}}{4} \left(\frac{\partial^2 \Psi_3}{\partial \zeta^2} - \frac{\partial^3 W_3}{\partial \zeta^3} \right), \tag{53a}$$

$$W_2 = W_3, d_{11} \frac{\partial \Psi_2}{\partial \zeta} + \frac{l_0^2 a_{55}}{4} \left(\frac{\partial \Psi_2}{\partial \zeta} - \frac{\partial^2 W_2}{\partial \zeta^2} \right) = d_{11} \frac{\partial \Psi_3}{\partial \zeta} + \frac{l_0^2 a_{55}}{4} \left(\frac{\partial \Psi_3}{\partial \zeta} - \frac{\partial^2 W_3}{\partial \zeta^2} \right), \tag{53b}$$

$$\frac{S_T}{A_{11} h} \left(\Psi_3 - \Psi_2 \right) = d_{11} \frac{\partial \Psi_3}{\partial \zeta} + \frac{l_0^2 a_{55}}{4} \left(\frac{\partial \Psi_3}{\partial \zeta} - \frac{\partial^2 W_3}{\partial \zeta^2} \right), \tag{53c}$$

$$\frac{l_0^2 a_{55}}{2} \left(\frac{\partial \Psi_2}{\partial \zeta} - \frac{\partial^2 W_2}{\partial \zeta^2} \right) = \frac{l_0^2 a_{55}}{2} \left(\frac{\partial \Psi_3}{\partial \zeta} - \frac{\partial^2 W_3}{\partial \zeta^2} \right), \frac{\partial W_2}{\partial \zeta} = \frac{\partial W_3}{\partial \zeta}. \tag{53d}$$

Since the beam is assumed to be infinitely long, there are no reflected waves at infinity on each side. As a result, $f_{21} = f_{41} = f_{61} = 0$ and $f_{13} = f_{33} = f_{53} = 0$. Thus, the vector of unknown coefficients is written as

$$\bar{\mathbf{f}} = \left(f_{11}, f_{31}, f_{51}, f_{12}, f_{22}, f_{32}, f_{42}, f_{52}, f_{62}, f_{23}, f_{43}, f_{63} \right)^{\mathrm{T}}. \tag{54}$$

Substituting Eqs. (51) and (52) into Eq. (53), we have

$$\bar{\mathbf{C}} \bar{\mathbf{f}} = \bar{\mathbf{Q}}, \tag{55}$$

where

$$\bar{\mathbf{C}}=\begin{bmatrix}
1 & 1 & 1 & -1 & -1 & -1 & -1 & -1 & -1 & 0 & 0 & 0\\
q_1 & q_2 & q_3 & -q_1 & q_1 & -q_2 & q_2 & -q_3 & q_3 & 0 & 0 & 0\\
k_1 & k_2 & k_3 & -k_1 & k_1 & -k_2 & k_2 & -k_3 & k_3 & 0 & 0 & 0\\
\gamma_{11} & \gamma_{21} & \gamma_{31} & -\gamma_{11} & \gamma_{11} & -\gamma_{21} & \gamma_{21} & -\gamma_{31} & \gamma_{31} & 0 & 0 & 0\\
\gamma_{12} & \gamma_{22} & \gamma_{32} & -\gamma_{12} & -\gamma_{12} & -\gamma_{22} & -\gamma_{22} & -\gamma_{32} & -\gamma_{32} & 0 & 0 & 0\\
\gamma_{13} & \gamma_{23} & \gamma_{33} & -\gamma_{13} & -\gamma_{13} & -\gamma_{23} & -\gamma_{23} & -\gamma_{33} & -\gamma_{33} & 0 & 0 & 0\\
0 & 0 & 0 & \gamma_{11}g_a & -\gamma_{11}/g_a & \gamma_{21}g_b & -\gamma_{21}/g_b & \gamma_{31}g_c & -\gamma_{31}/g_c & \gamma_{11} & \gamma_{21} & \gamma_{31}\\
0 & 0 & 0 & g_a & 1/g_a & g_b & 1/g_b & g_c & 1/g_c & -1 & -1 & -1\\
0 & 0 & 0 & -k_t q_1 g_a & k_t q_1/g_a & -k_t q_2 g_b & k_t q_2/g_b & -k_t q_3 g_c & k_t q_3/g_c & -k_t q_1-\gamma_{12} & -k_t q_2-\gamma_{22} & -k_t q_3-\gamma_{32}\\
0 & 0 & 0 & \gamma_{13}g_a & \gamma_{13}/g_a & \gamma_{23}g_b & \gamma_{23}/g_b & \gamma_{33}g_c & \gamma_{33}/g_c & -\gamma_{13} & -\gamma_{23} & -\gamma_{33}\\
0 & 0 & 0 & k_1 q_1 g_a & k_1 q_1/g_a & k_2 q_2 g_b & k_2 q_2/g_b & k_3 q_3 g_c & k_3 q_3/g_c & -k_1 q_1 & -k_2 q_2 & -k_3 q_3\\
0 & 0 & 0 & k_1 g_a & -k_1/g_a & k_2 g_b & -k_2/g_b & k_3 g_c & -k_3/g_c & k_1 & k_2 & k_3
\end{bmatrix},$$

$$\bar{\mathbf{Q}}=\left(0,0,0,F_0/A_{11},0,0,0,0,0,0,0,0\right)^{\mathrm{T}},$$

where the elements γ_{i1}, γ_{i2}, γ_{i3}, g_a, g_b, g_c in $\bar{\mathrm{C}}$ are given by,

$$k_t=\frac{S_T}{A_{11}h},\gamma_{i1}=k_s a_{55}\left(k_i+q_i\right)+\frac{l_0^2 a_{55}}{4}\left(k_i^2 q_i-k_i^3\right),$$

$$\gamma_{i2}=d_{11}k_i q_i+\frac{l_0^2 a_{55}}{4}\left(k_i q_i-k_i^2\right),\gamma_{i3}=k_i q_i-k_i^2,\left(i=1,2,3\right),$$

$$g_a=\mathrm{e}^{k_1 L_1},\ g_b=\mathrm{e}^{k_2 L_1},\ g_c=\mathrm{e}^{k_3 L_1}.$$

7. Vibrational power flow analysis

As a new measurement method of vibration intensity, the power flow has been widely concerned by scientists. In the vibration of structures, the existence of cracks disturbs the propagation path of original waves, which will change the vibrational power flow accordingly. By means of analyzing the changes of vibrational power flow, it can enable us to estimate the characteristics and distribution of cracks, and even for structural damage identification.

If the force and velocity of excitation accompanied by response are both in harmonic forms, the variations of force and velocity can be expressed as

$$\begin{aligned}F(t)&=\mathrm{Re}\left\{\tilde{F}\cdot\mathrm{e}^{\mathrm{i}\Omega t}\right\},\\ V(t)&=\mathrm{Re}\left\{\tilde{V}\cdot\mathrm{e}^{\mathrm{i}\Omega t}\right\}.\end{aligned}\tag{56}$$

The time-averaged power flow is given by

$$P=\frac{1}{T}\int_0^T \mathrm{Re}\left\{\tilde{F}\cdot \mathrm{e}^{\mathrm{i}\Omega t}\right\}\mathrm{Re}\left\{\tilde{V}\cdot \mathrm{e}^{\mathrm{i}\Omega t}\right\}\mathrm{d}t, \tag{57}$$

where $T=2\pi/\Omega$; $\tilde{F}$ and $\tilde{V}$ are complex numbers which contain the phase angle; (*) denotes the complex conjugate; (~) denotes the complex form. The real part and the imaginary part of $\tilde{F}$ and $\tilde{V}$ are expressed as

$$\begin{aligned}\tilde{F}&=F_a+\mathrm{i}F_b,\tilde{V}=V_a+\mathrm{i}V_b,\\ \tilde{F}^*&=F_a-\mathrm{i}F_b,\tilde{V}^*=V_a-\mathrm{i}V_b,\end{aligned} \tag{58}$$

where the subscripts "a" and "b" represent the real part and imaginary part, respectively. Therefore,

$$\begin{aligned}P&=\frac{1}{T}\int_0^T[F_a\cos\Omega t-F_b\sin\Omega t]\cdot[V_a\cos\Omega t-V_b\sin\Omega t]\mathrm{d}t\\ &=\frac{1}{2}\left(F_aV_a+F_bV_b\right)=\frac{1}{2}\mathrm{Re}\left\{\tilde{F}\cdot\tilde{V}^*\right\}=\frac{1}{2}\mathrm{Re}\left\{\tilde{F}^*\cdot\tilde{V}\right\}.\end{aligned} \tag{59}$$

Based on the conversion relation ($\tilde{V}=\mathrm{i}\Omega\tilde{Y}$) between displacement and velocity under the harmonic excitation, the time-averaged input power flow is given by

$$P_{in}=\frac{1}{2}\mathrm{Re}\left\{-\mathrm{i}\Omega\tilde{F}\tilde{Y}^*\right\}. \tag{60}$$

The input power flow is given by

$$P_{in}=\frac{1}{2}\mathrm{Re}\left\{-\mathrm{i}\Omega F_0\left|w\right|^*\right\}, \tag{61}$$

where (| • |) denotes the norm.

The transmitted power flow propagates in three forms: the shear force, couple moment and bending moment:

$$P_{tr}=\frac{1}{2}\mathrm{Re}\left\{-\mathrm{i}\Omega\left|M_y+\frac{1}{2}Y_{xy}\right|\cdot\left|\psi\right|^*\right\}+\frac{1}{2}\mathrm{Re}\left\{-\mathrm{i}\Omega\left|Q_z+\frac{1}{2}\frac{\partial Y_{xy}}{\partial x}\right|\cdot\left|w\right|^*\right\}+\frac{1}{2}\mathrm{Re}\left\{\mathrm{i}\Omega\frac{1}{2}\left|Y_{xy}\right|\cdot\left|\frac{\partial w}{\partial x}\right|^*\right\}. \tag{62}$$

Substituting Eqs. (17)-(19) into Eq. (62), the transmitted power flow is expressed as

$$P_{tr} = \frac{1}{2}\mathrm{Re}\left\{-\mathrm{i}\Omega\left|D_{11}\frac{\partial\psi}{\partial x}+\frac{1}{4}l^2A_{55}\left(\frac{\partial\psi}{\partial x}-\frac{\partial^2 w}{\partial x^2}\right)\right|\cdot|\psi|^*\right\}$$
$$+\frac{1}{2}\mathrm{Re}\left\{-\mathrm{i}\Omega\left|k_sA_{55}\left(\psi+\frac{\partial w}{\partial x}\right)+\frac{1}{4}l^2A_{55}\left(\frac{\partial^2\psi}{\partial x^2}-\frac{\partial^3 w}{\partial x^3}\right)\right|\cdot|w|^*\right\} \tag{63}$$
$$+\frac{1}{2}\mathrm{Re}\left[\mathrm{i}\Omega\frac{1}{4}l^2A_{55}\left|\frac{\partial\psi}{\partial x}-\frac{\partial^2 w}{\partial x^2}\right|\cdot\left|\frac{\partial w}{\partial x}\right|^*\right].$$

Substituting (47) or (48), (51) into Eqs. (61) and (63), the input and transmitted power flows of intact and cracked microbeams are derived which are showed in appendix A.

8. Numerical results

Both input and transmitted power flows of cracked microbeams are computed in this section. The beam is made of aluminum with the material properties: E = 70 GPa, ρ = 2780 kg/m^3 and υ = 0.33. Unless otherwise stated, the beam thickness takes h = 200 μm and the amplitude of the excitation force is F_0 = 1 N. The input and transmitted power flows are expressed in dimensionless forms of 10 log (P_{in} / F_0^2) and P_{tr} / P_{in} , respectively.

Up to now, to the best of the authors' knowledge, there is no research that has analyzed the vibrational power flow of microbeams. To verify the proposed microbeam model, we degrade our model to an isotropic homogeneous macroscale beam by setting the scale parameter as zero. The parameters of the cracked beam are given as: h = 0.1 m, E = 70 GPa, ρ = 2780 kg/m^3, F_0 = 100 N, L / h = 20 and a / h = 0.3. Fig. 4 compares the present results of the input power flow with the results obtained by Zhu et al. [17]. It shows a perfect agreement between Zhu et al.'s results and the present results.

8.1 Input power flow analysis

Fig. 5 shows the input power flow in both the intact and cracked microbeams, which have L / h = 100, a / h = 0.5 and h / l = 2. The frequency range of excitation varies from 1 Hz to 20000 Hz. The increase of excitation frequency leads to a decrease of the input power flow for both intact and cracked microbeams. It is observed that the crack does not significantly change the input power flow of the microbeam. Indeed, it is not observed the obvious fluctuation of the input power flow in cracked microbeams.

It had been well known that the change of the excitation frequency will lead to the fluctuation of the input power flow for macroscale cracked beams [17]. This is because the crack can interrupt the original wave

propagation path, that is, a part of traveling waves will be reflected when they meet the crack. This reflection wave results in a variation of the beam displacement at the excitation position, and in turn changes the characteristics of the input power flow. However, different with the macroscale cracked beam, the input power flow in cracked microbeams has barely fluctuation when the excitation frequency changes. To further study this fluctuation in input power flow, we introduce a value ε to quantify the difference of input power flow between intact and cracked beams:

$$\varepsilon = 10\left[\log_{10}\left(P_{in}^{i}/F_0^2\right) - \log_{10}\left(P_{in}^{c}/F_0^2\right)\right], \tag{64}$$

where P_{in}^{i} denotes the input power flow in an intact microbeam; P_{in}^{c} is the input power flow in a cracked microbeam. Fig. 6 presents the relation of the difference value ε versus the excitation frequency for the microbeam with a / h = 0.5 and h / l = 2. Interestingly, it is observed that the fluctuation of the difference value ε becomes clearly with the increase of frequency. Moreover, the fluctuation amplitude of ε is increased and the fluctuation frequency decreases with the increase of the excitation frequency.

Fig. 7 illustrates the influences of the scale parameter h / l on the input power flow (Fig. 7(a)) and the difference value ε (Fig. 7(b)) in cracked microbeams with L / h = 100 and a / h = 0.5. In Fig. 7(a), larger scale parameters lead to higher input power flows for a given frequency. As shown in Fig. 7(b), larger scale parameters will decrease the amplitude and the wavelength of the ε curve.

Fig. 8 shows the influences of the crack depth on the input power flow (Fig. 8(a)) and the difference value ε (Fig. 8(b)) in cracked microbeams with L / h = 100 and h / l = 2. In Fig. 8(a), it was found that the crack depth does not lead to any obvious change to the input power flow. As shown in Fig. 8(b), the increase of the crack depth leads to larger fluctuation amplitude of the ε curve. We can observe that there are many intersections among the ε curves with different crack depths, such as at 425Hz, 1706Hz, 3837Hz, 6820 Hz, 10652Hz and 15330Hz. At these intersection frequencies, one can conclude the power flow is not influenced by the variation of the crack depth due to ε = 0. However, the change of the crack depth does not affect the frequency of the ε curves.

Fig. 9 presents the influences of the crack location on the input power flow and the difference value ε in cracked microbeams with h / l = 2 and a / h = 0.5. The fluctuation frequency and amplitude of the ε curve are enlarged when the distance between the crack location and the excitation position increases.

Figs. 10-12 illustrate the correlation between the crack location and input power flow by considering different scale parameters, crack depths, crack locations and excitation frequencies, respectively. It was

observed in Figs. 10-12 that the input power flow with crack location L / h is a periodic fluctuant function. In Fig. 10, a larger scale parameter h / l will lead to a smaller input power flow for a given crack location. The increase of the scale parameter can cause the increase of the fluctuation amplitude and frequency. The increase of crack depth leads to the increase of the fluctuation amplitude of curves, as shown in Fig. 11. Interestingly, the crack depth does not affect the frequency of curves, as illustrated by Fig. 11. In Fig. 12, a larger driving frequency will lead to a smaller input power flow for a given crack location. The increase of the excitation frequency causes the increase of the fluctuation amplitude and frequency of the curve.

8.2 Transmitted power flow analysis

Fig. 13 shows the influence of the scale parameter h / l on the transmitted power flow P_{tr} / P_{in} in the cracked microbeams with $L / h = 100$ and $a / h = 0.5$. Different with the input power flow, the transmitted power flow exhibits the fluctuation much obviously. It is found that a large scale parameter will lead to the decrease of the amplitude and wavelength of the transmitted power flow curve.

Fig. 14 presents the influence of the crack depth on the transmitted power flow P_{tr} / P_{in} in cracked microbeam with $L / h = 100$ and $h / l = 2$. The transmitted power flow P_{tr} / P_{in} remains unchanged at 0.5 for an intact microbeam. It implies that the energy input into the microbeam from the external excitation is equally divided according to the direction of propagation. The transmitted power flow curves of the cracked microbeam fluctuate around the constant 0.5 of the intact microbeam. The amplitude of the curves increases with the increase of the crack depth. The crack depth does not affect the wave frequencies of transmitted power flow, as illustrated by cracked curves. Similar with the input power flow, the transmitted power flow is not influenced by the crack depth at some frequencies, such as 425Hz, 1706Hz, 3837Hz, 6820 Hz, 10652Hz and 15330Hz.

The influences of the crack location on the transmitted power flow in cracked microbeams with $a / h = 0.5$ and $h / l = 2$ are shown in Fig. 15. The crack location has a significant influence on the transmitted power flow. It is indicated that the increase of the crack location leads to the increase of fluctuation frequency of transmitted power flow curves.

Figs. 16-18 show the influences of the scale parameters, the excitation frequencies, and the crack depths on the curves of transmitted power flow *vs.* crack location, respectively. It is revealed that the transmitted power flow is a periodic function as the same with the input power flow. As shown in Fig. 16, the increase of the scale parameter pulls down the amplitude and wavelength of transmitted power flow curves. Fig. 17 shows

that the increase of the crack depth leads to the increase of the amplitude of transmitted power flow curves. In Fig. 18, the increase of the frequency enlarges the amplitude of transmitted power flow curves, while reduces the wavelength of transmitted power flow curves.

9. Conclusions

In this paper, an analytical model is developed for the analysis of vibrational power flow in cracked microbeams based on the Timoshenko beam theory and modified couple stress theory. The crack is modelled as a rotational spring, the stiffness of which is determined using the stress intensity factors. The vibrational response of a cracked microbeam under a transverse harmonic excitation is solved by the wave propagation method. The influences of the scale parameter, the crack location and the crack depth on the input and transmitted power flows are discussed. The following points are arrived from our simulation and analysis:

(1) The input and transmitted power flows are the periodic functions with respect to the crack location.

(2) The input power flow of cracked microbeams has barely fluctuations with the variation of the excitation frequency. However, the difference value ε of the input power flow between intact and cracked microbeams exhibits obvious fluctuations.

(3) The transmitted power flow of cracked microbeams exhibits the obvious fluctuation.

(4) A large scale parameter will lead to the decrease of the amplitude and wavelength of transmitted power flow curves.

(5) With the increase of the crack depth, the amplitude of the transmitted power flow curve increases, while it does not affect the wavelength of curves.

Acknowledgments

This work is funded by the National Natural Science Foundation of China (Nos. 11725207 and 12021002).

Appendix A. Expression of power flow

For intact beam

$$P_{in}\big|_{\varsigma=0} = \frac{1}{2}\mathrm{Re}\left\{-\mathrm{i}\Omega F_0 h(f_{11} + f_{31} + f_{51})^*\right\},$$

$$P_{tr}\big|_{\varsigma} = \frac{1}{2}\mathrm{Re}\left\{-\mathrm{i}\Omega\left[\frac{D_{11}}{h}\psi_L^{(1)} + \frac{l^2 A_{55}}{4h}\left(\psi_L^{(1)} - w_L^{(2)}\right)\right]\cdot\psi_L^{(0)*}\right\} + \frac{1}{2}\mathrm{Re}\left\{\mathrm{i}\Omega\frac{l^2 A_{55}}{4h}\left(\psi_L^{(1)} - w_L^{(2)}\right)\cdot w_L^{(1)*}\right\}$$

$$+\frac{1}{2}\mathrm{Re}\left\{-\mathrm{i}\Omega\left[k_s A_{55}\left(\psi_L^{(0)} + w_L^{(1)}\right) + \frac{l^2 A_{55}}{4h^2}\left(\psi_L^{(2)} - w_L^{(3)}\right)\right]\cdot w_L^{(0)*}\right\},$$

for $\zeta \le 0$ and

$$P_{tr}\big|_{\varsigma} = \frac{1}{2}\mathrm{Re}\left\{-\mathrm{i}\Omega\left[\frac{D_{11}}{h}\psi_R^{(1)} + \frac{l^2 A_{55}}{4h}\left(\psi_R^{(1)} - w_R^{(2)}\right)\right]\cdot\psi_R^{(0)*}\right\} + \frac{1}{2}\mathrm{Re}\left\{\mathrm{i}\Omega\frac{l^2 A_{55}}{4h}\left(\psi_R^{(1)} - w_R^{(2)}\right)\cdot w_R^{(1)*}\right\}$$

$$+\frac{1}{2}\mathrm{Re}\left\{-\mathrm{i}\Omega\left[k_s A_{55}\left(\psi_R^{(0)} + w_R^{(1)}\right) + \frac{l^2 A_{55}}{4h^2}\left(\psi_R^{(2)} - w_R^{(3)}\right)\right]\cdot w_R^{(0)*}\right\},$$

for $\zeta > 0$, where

$$\psi_L^{(0)} = q_1 f_{11} g_a + q_2 f_{31} g_b + q_3 f_{51} g_c;\ \ \psi_L^{(1)} = q_1 f_{11} k_1 g_a + q_2 f_{31} k_2 g_b + q_3 f_{51} k_3 g_c;$$

$$\psi_L^{(2)} = q_1 f_{11} k_1^2 g_a + q_2 f_{31} k_2^2 g_b + q_3 f_{51} k_3^2 g_c;$$

$$w_L^{(0)} = f_{11} g_a + f_{31} g_b + f_{51} g_c; w_L^{(1)} = f_{11} k_1 g_a + f_{31} k_2 g_b + f_{51} k_3 g_c;$$
$$w_L^{(2)} = f_{11} k_1^2 g_a + f_{31} k_2^2 g_b + f_{51} k_3^2 g_c;\ w_L^{(3)} = f_{11} k_1^3 g_a + f_{31} k_2^3 g_b + f_{51} k_3^3 g_c;$$

$$\psi_R^{(0)} = -q_1 f_{22} g_a^{-1} - q_2 f_{42} g_b^{-1} - q_3 f_{62} g_c^{-1};\ \ \psi_R^{(1)} = q_1 f_{22} k_1 g_a^{-1} + q_2 f_{42} k_2 g_b^{-1} + q_3 f_{62} k_3 g_c^{-1};$$

$$\psi_R^{(2)} = -q_1 f_{22} k_1^2 g_a^{-1} - q_2 f_{42} k_2^2 g_b^{-1} - q_3 f_{62} k_3^2 g_c^{-1};$$

$$w_R^{(0)} = f_{22} g_a^{-1} + f_{42} g_b^{-1} + f_{62} g_c^{-1};\ w_R^{(1)} = -f_{22} k_1 g_a^{-1} - f_{42} k_2 g_b^{-1} - f_{62} k_3 g_c^{-1};$$
$$w_R^{(2)} = f_{22} k_1^2 g_a^{-1} + f_{42} k_2^2 g_b^{-1} + f_{62} k_3^2 g_c^{-1};\ w_R^{(3)} = -f_{22} k_1^3 g_a^{-1} - f_{42} k_2^3 g_b^{-1} - f_{62} k_3^3 g_c^{-1}.$$

For cracked beam

$$P_{in}\big|_{\varsigma=0} = \frac{1}{2}\mathrm{Re}\left\{-\mathrm{i}\Omega F_0 h(f_{11} + f_{31} + f_{51})^*\right\},$$

$$P_{tr}\big|_{\varsigma} = \frac{1}{2}\mathrm{Re}\left\{-\mathrm{i}\Omega\left[\frac{D_{11}}{h}\hat{\psi}_L^{(1)} + \frac{l^2 A_{55}}{4h}\left(\hat{\psi}_L^{(1)} - \hat{w}_L^{(2)}\right)\right]\cdot\hat{\psi}_L^{(0)*}\right\} + \frac{1}{2}\mathrm{Re}\left\{\mathrm{i}\Omega\frac{l^2 A_{55}}{4h}\left(\hat{\psi}_L^{(1)} - \hat{w}_L^{(2)}\right)\cdot\hat{w}_L^{(1)*}\right\}$$

$$+\frac{1}{2}\mathrm{Re}\left\{-\mathrm{i}\Omega\left[k_s A_{55}\left(\hat{\psi}_L^{(0)} + \hat{w}_L^{(1)}\right) + \frac{l^2 A_{55}}{4h^2}\left(\hat{\psi}_L^{(2)} - \hat{w}_L^{(3)}\right)\right]\cdot\hat{w}_L^{(0)*}\right\},$$

for $\zeta \le 0$ and

$$P_{tr}\big|_{\varsigma}=\frac{1}{2}\mathrm{Re}\left\{-\mathrm{i}\Omega\left[\frac{D_{11}}{h}\hat{\psi}_M^{(1)}+\frac{l^2A_{55}}{4h}\left(\hat{\psi}_M^{(1)}-\hat{w}_M^{(2)}\right)\right]\cdot\hat{\psi}_M^{(0)*}\right\}+\frac{1}{2}\mathrm{Re}\left\{\mathrm{i}\Omega\frac{l^2A_{55}}{4h}\left(\hat{\psi}_M^{(1)}-\hat{w}_M^{(2)}\right)\cdot\hat{w}_M^{(1)*}\right\}$$

$$+\frac{1}{2}\mathrm{Re}\left\{-\mathrm{i}\Omega\left[k_sA_{55}\left(\hat{\psi}_M^{(0)}+\hat{w}_M^{(1)}\right)+\frac{l^2A_{55}}{4h^2}\left(\hat{\psi}_M^{(2)}-\hat{w}_M^{(3)}\right)\right]\cdot\hat{w}_M^{(0)*}\right\},$$

for $0\le\zeta\le L_1$ and

$$P_{tr}\big|_{\varsigma}=\frac{1}{2}\mathrm{Re}\left\{-\mathrm{i}\Omega\left[\frac{D_{11}}{h}\hat{\psi}_R^{(1)}+\frac{l^2A_{55}}{4h}\left(\hat{\psi}_R^{(1)}-\hat{w}_R^{(2)}\right)\right]\cdot\hat{\psi}_R^{(0)*}\right\}+\frac{1}{2}\mathrm{Re}\left\{\mathrm{i}\Omega\frac{l^2A_{55}}{4h}\left(\hat{\psi}_R^{(1)}-\hat{w}_R^{(2)}\right)\cdot\hat{w}_R^{(1)*}\right\}$$

$$+\frac{1}{2}\mathrm{Re}\left\{-\mathrm{i}\Omega\left[k_sA_{55}\left(\hat{\psi}_R^{(0)}+\hat{w}_R^{(1)}\right)+\frac{l^2A_{55}}{4h^2}\left(\hat{\psi}_R^{(2)}-\hat{w}_R^{(3)}\right)\right]\cdot\hat{w}_R^{(0)*}\right\},$$

for $\zeta> L_1$, where

$$\hat{\psi}_L^{(0)}=q_1f_{11}g_a+q_2f_{31}g_b+q_3f_{51}g_c;\ \hat{\psi}_L^{(1)}=q_1f_{11}k_1g_a+q_2f_{31}k_2g_b+q_3f_{51}k_3g_c;$$
$$\hat{\psi}_L^{(2)}=q_1f_{11}k_1^2g_a+q_2f_{31}k_2^2g_b+q_3f_{51}k_3^2g_c;$$

$$\hat{w}_L^{(0)}=f_{11}g_a+f_{31}g_b+f_{51}g_c;\ \hat{w}_L^{(1)}=f_{11}k_1g_a+f_{31}k_2g_b+f_{51}k_3g_c;$$
$$\hat{w}_L^{(2)}=f_{11}k_1^2g_a+f_{31}k_2^2g_b+f_{51}k_3^2g_c;\ \hat{w}_L^{(3)}=f_{11}k_1^3g_a+f_{31}k_2^3g_b+f_{51}k_3^3g_c;$$

$$\hat{\psi}_M^{(0)}=q_1f_{12}g_a-q_1f_{22}g_a^{-1}+q_2f_{32}g_b-q_2f_{42}g_b^{-1}+q_3f_{52}g_c-q_3f_{62}g_c^{-1};$$
$$\hat{\psi}_M^{(1)}=q_1f_{12}k_1g_a+q_1f_{22}k_1g_a^{-1}+q_2f_{32}k_2g_b+q_2f_{42}k_2g_b^{-1}+q_3f_{52}k_3g_c+q_3f_{62}k_3g_c^{-1};$$
$$\hat{\psi}_M^{(2)}=q_1f_{12}k_1^2g_a-q_1f_{22}k_1^2g_a^{-1}+q_2f_{32}k_2^2g_b-q_2f_{42}k_2^2g_b^{-1}+q_3f_{52}k_3^2g_c-q_3f_{62}k_3^2g_c^{-1};$$

$$\hat{w}_M^{(0)}=f_{12}g_a+f_{22}g_a^{-1}+f_{32}g_b+f_{42}g_b^{-1}+f_{52}g_c+f_{62}g_c^{-1};$$
$$\hat{w}_M^{(1)}=f_{12}k_1g_a-f_{22}k_1g_a^{-1}+f_{32}k_2g_b-f_{42}k_2g_b^{-1}+f_{52}k_3g_c-f_{62}k_3g_c^{-1};$$
$$\hat{w}_M^{(2)}=f_{12}k_1^2g_a+f_{22}k_1^2g_a^{-1}+f_{32}k_2^2g_b+f_{42}k_2^2g_b^{-1}+f_{52}k_3^2g_c+f_{62}k_3^2g_c^{-1};$$
$$\hat{w}_M^{(3)}=f_{12}k_1^3g_a-f_{22}k_1^3g_a^{-1}+f_{32}k_2^3g_b-f_{42}k_2^3g_b^{-1}+f_{52}k_3^3g_c-f_{62}k_3^3g_c^{-1};$$

$$\hat{w}_R^{(0)}=f_{23}g_a^{-1}+f_{43}g_b^{-1}+f_{63}g_c^{-1};\ \hat{w}_R^{(1)}=-f_{23}k_1g_a^{-1}-f_{43}k_2g_b^{-1}-f_{63}k_3g_c^{-1};$$
$$\hat{w}_R^{(2)}=f_{23}k_1^2g_a^{-1}+f_{43}k_2^2g_b^{-1}+f_{63}k_3^2g_c^{-1};\ \hat{w}_R^{(3)}=-f_{23}k_1^3g_a^{-1}-f_{43}k_2^3g_b^{-1}-f_{63}k_3^3g_c^{-1}.$$

$$\hat{w}_R^{(0)}=f_{23}g_a^{-1}+f_{43}g_b^{-1}+f_{63}g_c^{-1};\ \hat{w}_R^{(1)}=-f_{23}k_1g_a^{-1}-f_{43}k_2g_b^{-1}-f_{63}k_3g_c^{-1};$$
$$\hat{w}_R^{(2)}=f_{23}k_1^2g_a^{-1}+f_{43}k_2^2g_b^{-1}+f_{63}k_3^2g_c^{-1};\ \hat{w}_R^{(3)}=-f_{23}k_1^3g_a^{-1}-f_{43}k_2^3g_b^{-1}-f_{63}k_3^3g_c^{-1}.$$

References

1. Bahrami. Free vibration, wave power transmission and reflection in multi-cracked nanorods. Compos Part B-Eng 2017;127:53-62.
2. S. M. Mousavi Janbeh Sarayi, A. Bahrami, M. N. Bahrami. Free vibration and wave power reflection in Mindlin rectangular plates via exact wave propagation approach. Compos Part B-Eng 2018;144:195-205.
3. S. T. Deng, J. Pang, Z. Zhang, L. Yang, X. Q. Li, H. L. Dai. Investigation on characteristics of energy transfer of flexural vibration in a Y-shaped bifurcated beam imposed lumped mass. Appl Math Model 2021;92:486-504.
4. M. Ghavami, S. Azizi, M. R. Ghazavi. On the dynamics of a capacitive electret-based micro-cantilever for energy harvesting. Energy 2018;153:967-976.
5. S. Nabavi, L. H. Zhang. Frequency tuning and efficiency Improvement of piezoelectric MEMS vibration energy harvesters. J Microelectromech S 2019;28(1):77-87.
6. Y. Wang, X. Y. Liu, T. Y. Chen, H. Wang, C. Q. Zhu, H. Y. Yu, L. G. Song, X. X. Pan, J. C. Mi, C. K. Lee, M. Y. Xu. An underwater flag-like triboelectric nanogenerator for harvesting ocean current energy under extremely low velocity condition. Nano Energy 2021;90:106503.
7. J. X. Liu, W. T. He, D. Xie. Study on vibrational power flow propagation characteristics in a laminated composite cylindrical shell filled with fluid. Shock Vib 2018;2018:1-19.
8. D. S. Cho, T. M. Choi, J. H. Kim, N. Vladimir. Dominant components of vibrational energy flow in stiffened panels analyzed by the structural intensity technique. Int J Nav Arch Ocean 2018;10(5):583-595.
9. Z. H. Liu, J. C. Niu. Vibrational energy flow model for functionally graded beams. Compos Struct 2018;186:17-28.
10. M. Sheng, T. Wang, M. Wang, X. Wang, X. Zhao. Effect of distributive mass of spring on power flow in engineering test. J Sound Vib 2018;424:365-377.
11. X. Zheng, W. Dai, Y. Qiu, Z. Hao. Prediction and energy contribution analysis of interior noise in a high-speed train based on modified energy finite element analysis. Mech Syst Signal Pr 2019;126:439–457.
12. L. Wang, T. Chen. Structural intensity analysis of the cantilevered plate under thermal load. Thin Wall Struct 2019;139:209–218.
13. Y. Q. Ma, Q. J. Zhao, K. Zhang, M. Xu, W. Zhao. Effects of mount positions on vibrational energy flow transmission characteristics in aero-engine casing structures. J Low Freq Noise V A 2020;39(2):313-326.

14. T. Y. Li, J. X. Liu, T. Zhang. Vibrational power flow characteristics of circular plate structures with peripheral surface crack. J Sound Vib 2004;276(3-5):1081-1091.
15. X. Zhu, T. Y. Li, Y. Zhao, J. Yan. Vibrational power flow analysis of thin cylindrical shell with a circumferential surface crack. J Sound Vib 2007;302(1-2):332-349.
16. H. L. Xu, Z. S. Chen, Y. P. Xiong, Y. M. Yang, L. M. Tao. Nonlinear dynamic behaviors of rotated blades with small breathing cracks based on vibration power flow analysis. Shock Vib 2016;2016(1):1-11.
17. L. F. Zhu, L. L. Ke, Y. Xiang, X. Q. Zhu, Y. S. Wang. Vibrational power flow analysis of cracked functionally graded beams. Thin Wall Struct 2020;150:106626.
18. S. H. Zheng, Y. K. Yu, M. Z. Qiu, L. M. Wang, D. P. Tan. A modal analysis of vibration response of a cracked fluid-filled cylindrical shell. Appl Math Model 2021;91: 934-958.
19. F. Yang, A. C. M. Chong, D. C. C. Lam, P. Dong. Couple stress based strain gradient theory for elasticity. Int J Solids Struct 2002;39(10):2731-2743.
20. H. M. Ma, X. L. Gao, J. N. Reddy. A microstructure-dependent Timoshenko beam model based on a modified couple stress theory. J Mech Phys Solids 2008;56(12):3379-3391.
21. L. L. Ke, Y. S. Wang. Size effect on dynamic stability of functionally graded microbeams based on a modified couple stress theory. Compos Struct 2011;93(2):342-350.
22. J. Ehyaei, M. R. Akbarizadeh. Vibration analysis of micro composite thin beam based on modified couple stress. Struct Eng Mech 2017;64(4):403-411.
23. R. Abbas. Vibration analysis of multiple-layer microbeams based on the modified couple stress theory: analytical approach. Arch Appl Mech 2021;91(1):23-32.
24. A. E. Giannakopoulos, K. Stamoulis. Structural analysis of gradient elastic components. Int J Solids Struct 2007;44(10):3440-3451.
25. X. Zhao, W. D. Zhu, Y. H. Li. Analytical solutions of nonlocal coupled thermoelastic forced vibrations of micro-/nano-beams by means of Green's functions. J Sound Vib 2020;481:115407.
26. R. Kumar, R. Kumar. Effect of two-temperature parameter on thermoelastic vibration in micro and nano beam resonator. Eur J Mech A-Solid 2021;89:104310.
27. S. Hosseini-Hashemi, M. Zare, R. Nazemnezhad. An exact analytical approach for free vibration of Mindlin rectangular nano-plates via nonlocal elasticity. Compos Struct 2013;100:290-299.
28. H. Salehipour, A. Shahsavar. A three-dimensional elasticity model for free vibration analysis of

functionally graded micro/nano plates: modified strain gradient theory. Compos Struct 2018;206:415-424.

29. J. Kim, K. K. Zur, J. N. Reddy. Bending, free vibration, and buckling of modified couples stress-based functionally graded porous micro-plates. Compos Struct 2019;209:879-888.
30. M. Arefi, M. Kiani, A. M. Zenkour. Size-dependent free vibration analysis of a three-layered exponentially graded nano-/micro-plate with piezomagnetic face sheets resting on Pasternak's foundation via MCST. J Sandw Struct Mater 2020;22(1):55-86.
31. S. Amir, E. Arshid, S. M. A. Rasti-Alhosseini, A. Loghman. Quasi-3D tangential shear deformation theory for size-dependent free vibration analysis of three-layered FG porous micro rectangular plate integrated by nano-composite faces in hygrothermal environment. J Therm Stresses 2020;43(2):133-156.
32. X. P. Zhou, L. Wang. Vibration and stability of micro-scale cylindrical shells conveying fluid based on modified couple stress theory. Micro Nano Lett 2012;7(7):679-684.
33. R. Gholami, A. Darvizeh, R. Ansari, F. Sadeghi. Vibration and buckling of first-order shear deformable circular cylindrical micro-/nano-shells based on Mindlin's strain gradient elasticity theory. Eur J Mech A-Solid 2016;58:76-88.
34. A. R. Ghasemi, M. Mohandes. Free vibration analysis of micro and nano fiber-metal laminates circular cylindrical shells based on modified couple stress theory. Mech Adv Mater Struc 2018;27(1):1-12.
35. R. Sourki, S. A. H. Hoseini. Free vibration analysis of size-dependent cracked microbeam based on the modified couple stress theory. Appl Phys A-Mater 2016;122(4):413.
36. A. Rahi. Crack mathematical modeling to study the vibration analysis of cracked micro beams based on the MCST. Microsyst Technol 2018;24(7):3201-3215.
37. H. Zhou, W. M. Zhang, Z. K. Peng, G. Meng. Dynamic characteristics of electrostatically actuated microbeams with slant crack. Math Probl Eng 2015;2015:208065.
38. S. D. Akbas. Forced vibration analysis of cracked functionally graded microbeams. Adv Nano Res 2018;6(1)39-55.
39. S. Ziaee. Linear free vibration of micro-/nano-plates with cut-out in thermal environment via modified couple stress theory and Ritz method. Ain Shams Eng J 2018;9(4):2373-2381.
40. A. Bahrami, A. Teimourian. Study on the effect of small scale on the wave reflection in carbon nanotubes using nonlocal Timoshenko beam theory and wave propagation approach. Compos Part B-Eng 2016;91:492-504.

41. A. Bahrami, A. Teimourian. Nonlocal scale effects on buckling, vibration and wave reflection in nanobeams via wave propagation approach. Compos Struct 2015;134:1061-1075.
42. A. Bahrami, A. Teimourian. Small scale effect on vibration and wave power reflection in circular annular nanoplates. Compos Part B-Eng 2017;109:214-226.
43. A. Bahrami. A wave-based computational method for free vibration, wave power transmission and reflection in multi-cracked nanobeams. Compos Part B-Eng 2017;120:168-181.
44. A. Bahrami. Free vibration, wave power transmission and reflection in multi-cracked nanorods. Compos Part B-Eng 2017;127:53-62.
45. M. R. Ilkhani, A. Bahrami, S. H. Hosseini-Hashemi. Free vibrations of thin rectangular nano-plates using wave propagation approach. Appl Math Model 2016;40:1287-1299.
46. F. Ebrahimi, K. Khosravi, A. Dabbagh. A novel spatial-temporal nonlocal strain gradient theorem for wave dispersion characteristics of FGM nanoplates. Wave Random Complex 2021;doi: 10.1080/17455030.2021.1979272.
47. H. Zeighampour, Y. T. Beni, I. Karimipour. Wave propagation in double-walled carbon nanotube conveying fluid considering slip boundary condition and shell model based on nonlocal strain gradient theory. Microfluid Nanofluid 2017;21(5):85.
48. S. G. Lekhnitsii. Anisotropic plates. Gordon and Breach Science Publishers 1968.

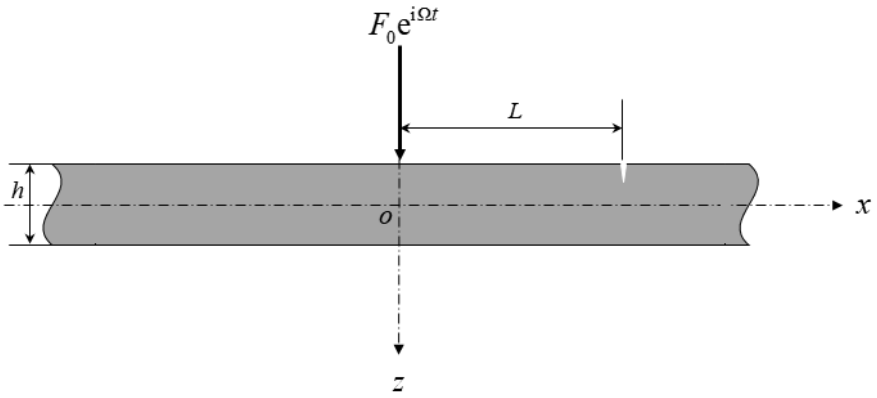

Fig. 1. A cracked microbeam subjected to an excitation force.

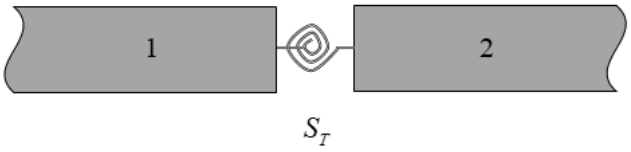

Fig. 2. The massless elastic rotational spring model.

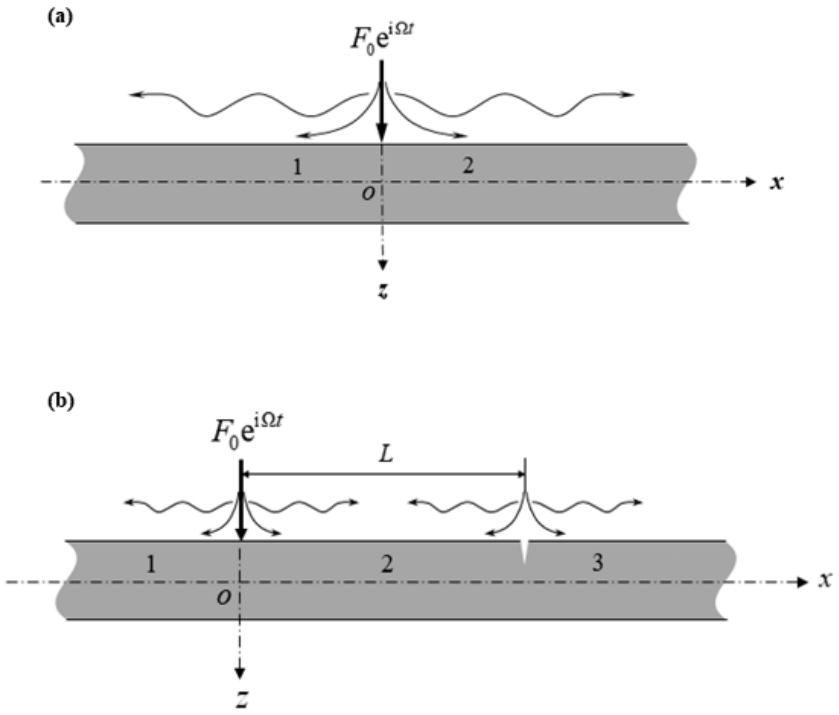

Fig. 3. The propagating and evanescent waves under a harmonic excitation in a microbeam without a crack (a) and with a crack (b).

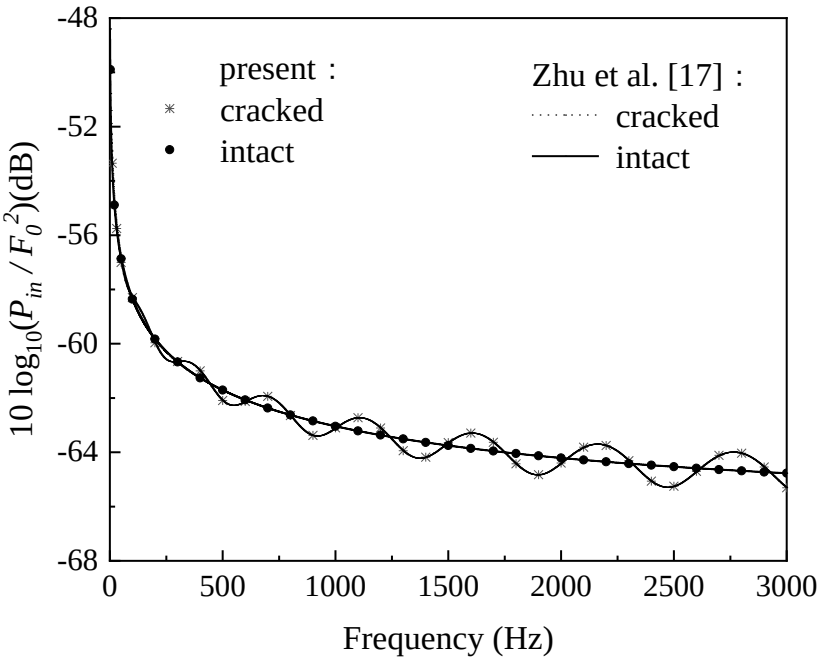

Fig. 4. The relation between the input power flow and frequency for the intact and cracked macrobeams.

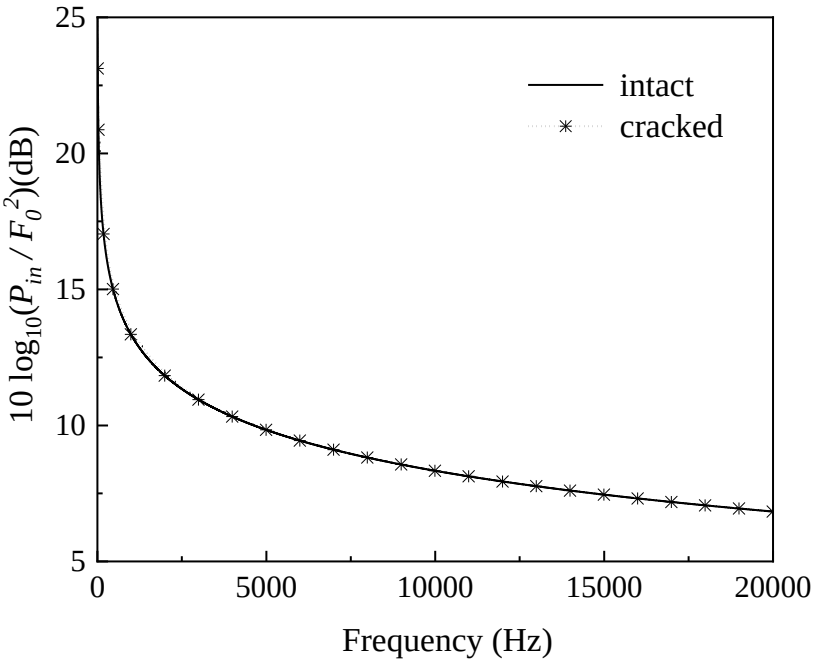

Fig. 5. The relation between the input power flow and frequency for microbeams with $L / h = 100$, $a / h = 0.5$ and $h / l = 2$.

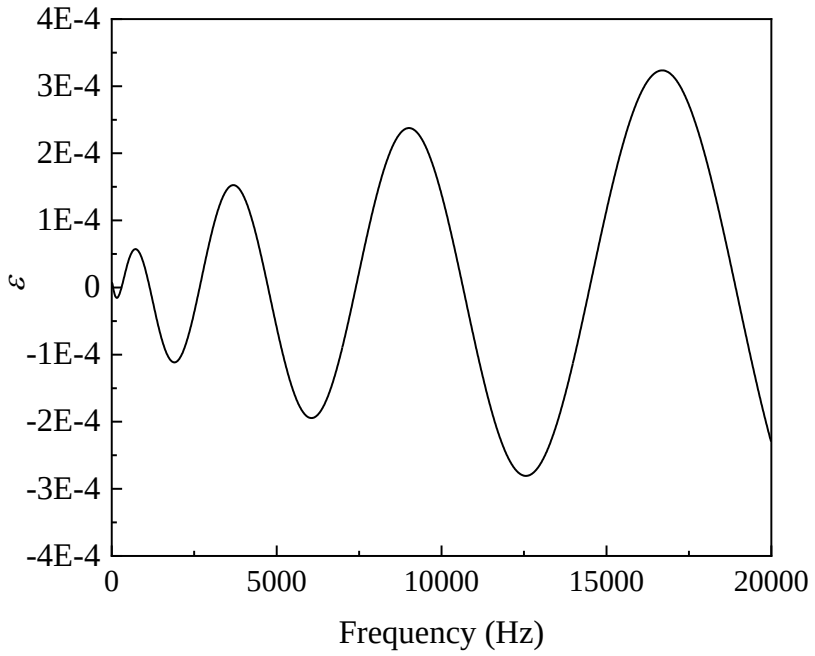

Fig. 6. The difference value ε of the input power flow between intact and cracked microbeams with L / h = 100, a / h = 0.5 and h / l = 2.

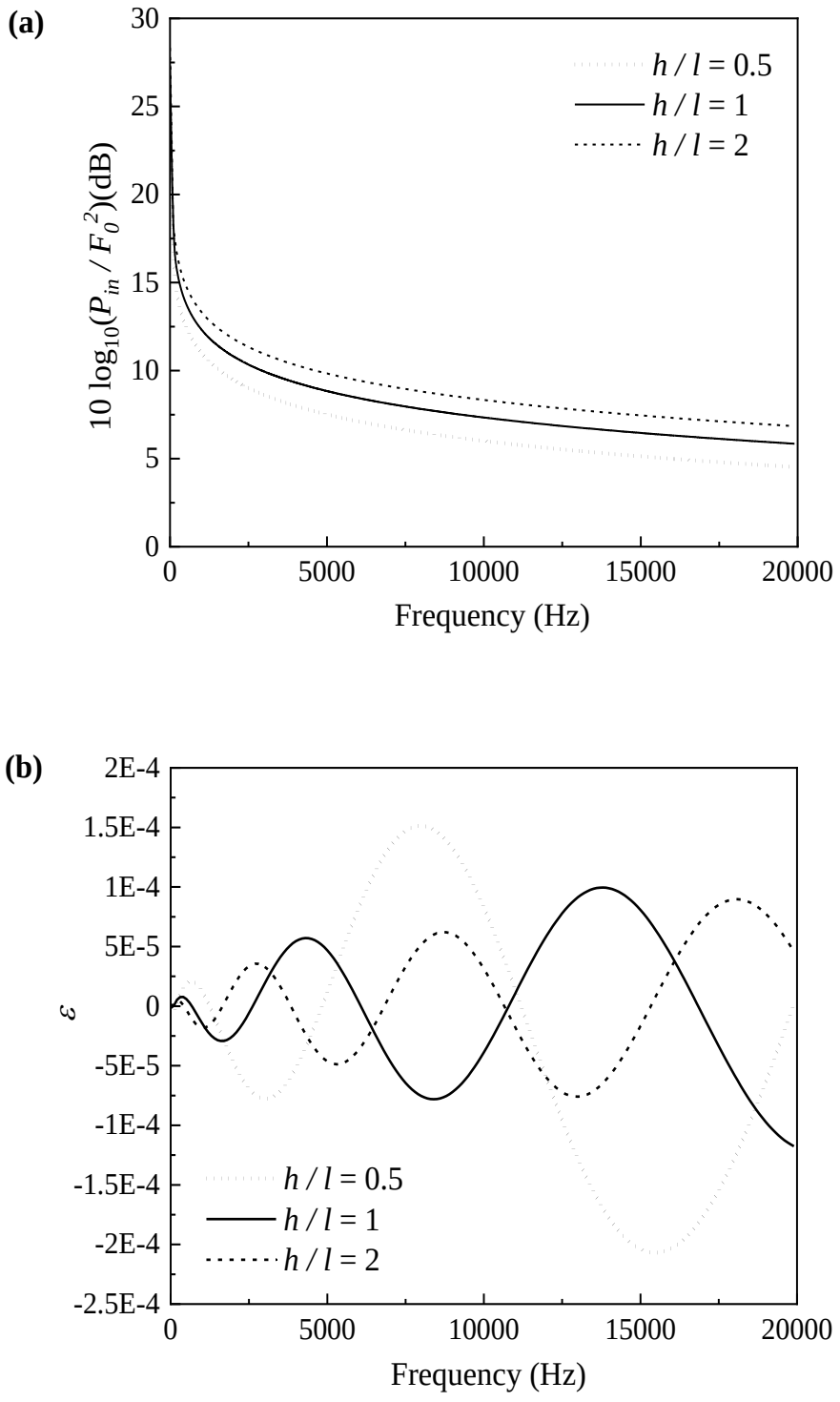

Fig. 7. Influence of h / l on the input power flow (a) and ε (b) versus frequency curves of cracked microbeams with $a / h = 0.5$ and $L / h = 100$.

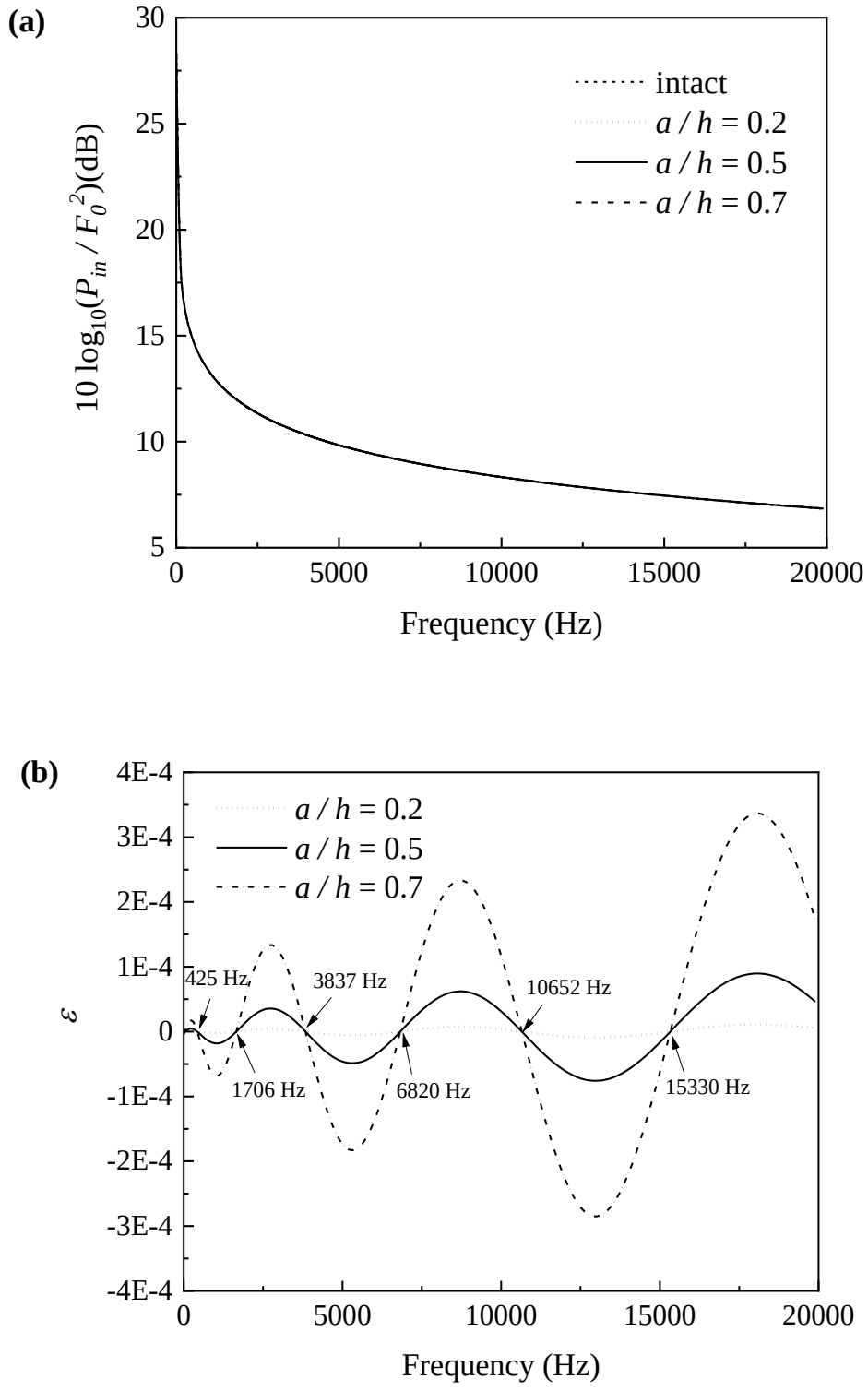

Fig. 8. Influence of *a*/ *h* on the input power flow (a) and ε (b) versus frequency curves of cracked microbeams with $L / h = 100$ and $h / l = 2$.

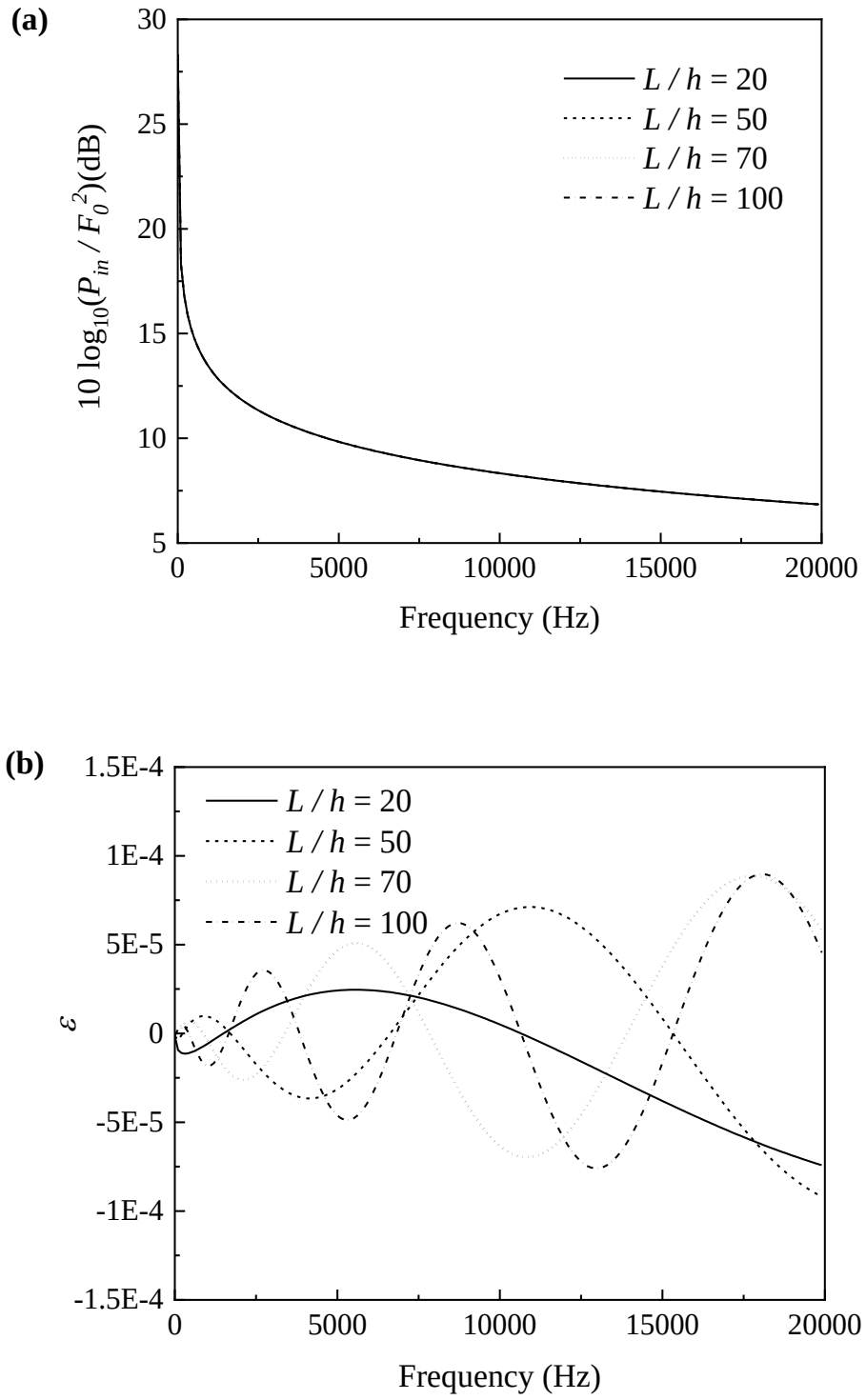

Fig. 9. Influence of L / h on the input power flow (a) and ε (b) versus frequency curves of cracked microbeams with $h / l = 2$ and $a / h = 0.5$.

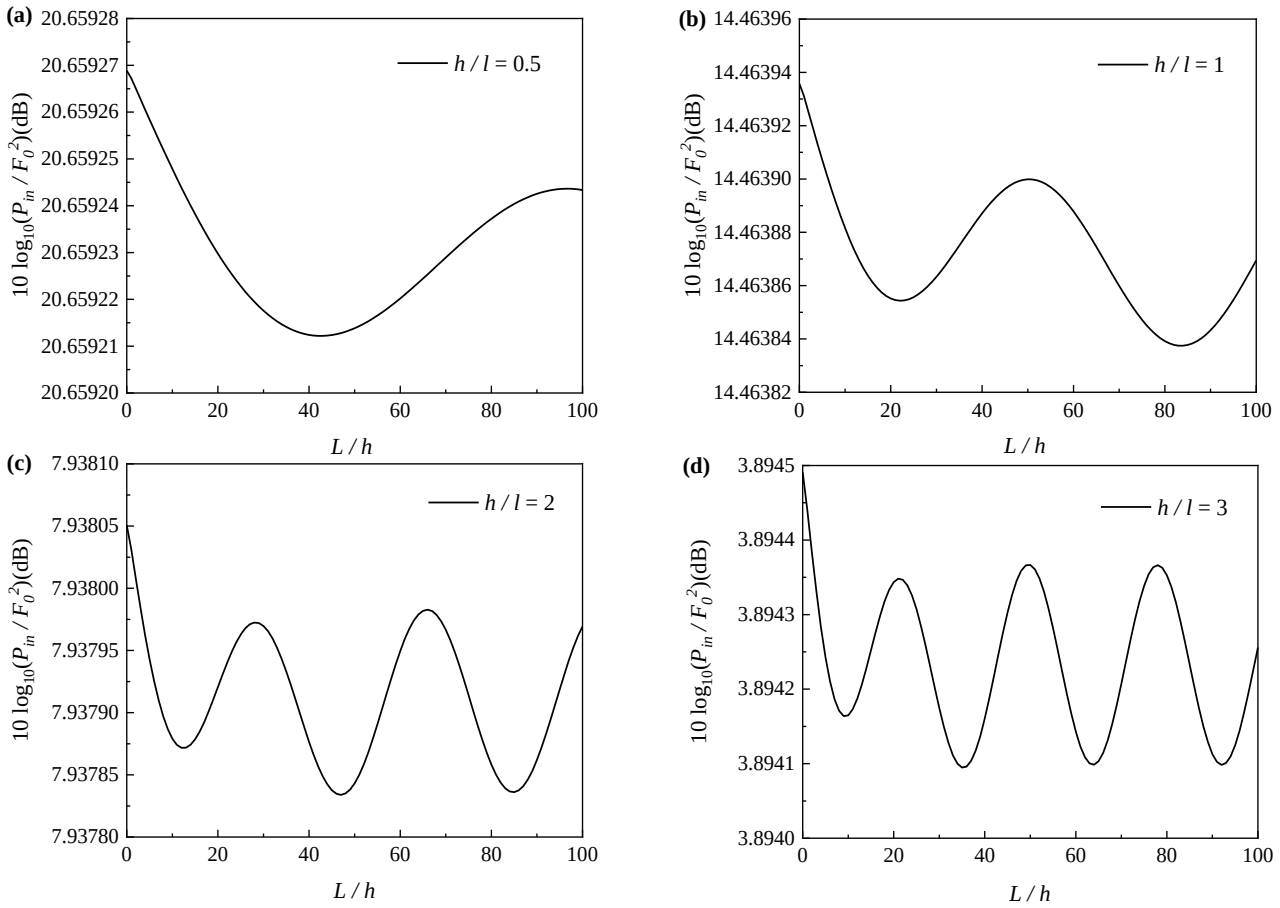

Fig. 10. Influence of h / l on the input power flow versus crack location curves of cracked microbeams with f = 12000 Hz and a / h = 0.5: h / l = 0.5 (a), h / l = 1 (b), h / l = 2 (c) and h / l = 3 (d).

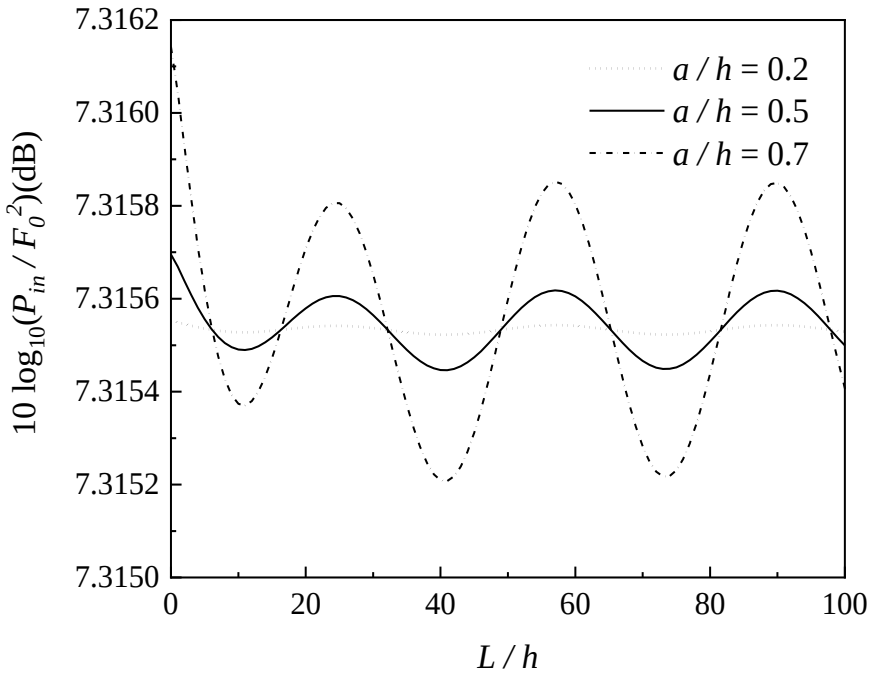

Fig. 11. Influence of a/h on the input power flow versus crack location curves with f = 12000 Hz and h/l = 2.

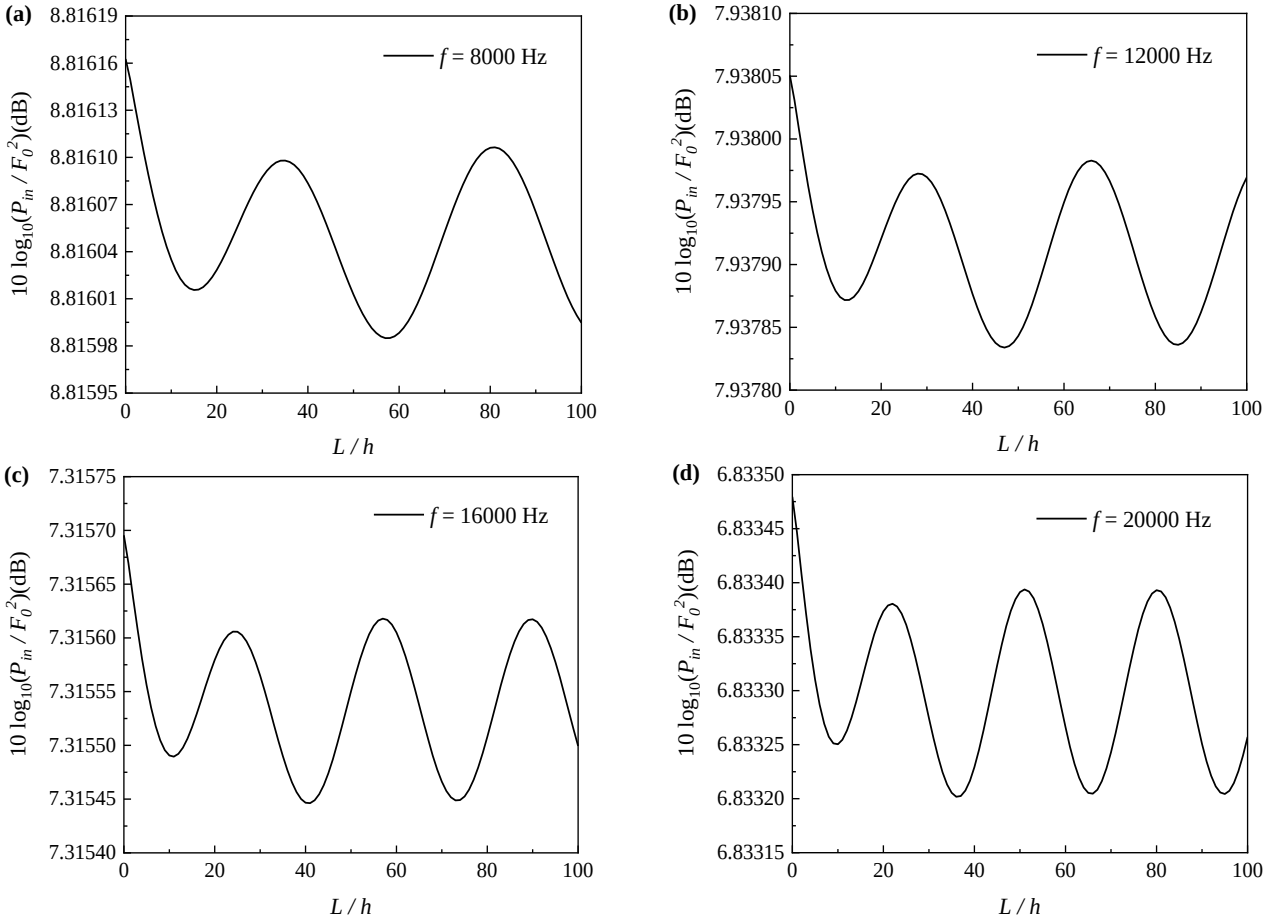

Fig. 12. Influence of f on the input power flow versus crack location curves with $h / l = 2$ and $a / h = 0.5$: $f =$ 8000 Hz (a), $f = 12000$ Hz (b), $f = 16000$ Hz (c) and $f = 20000$ Hz (d).

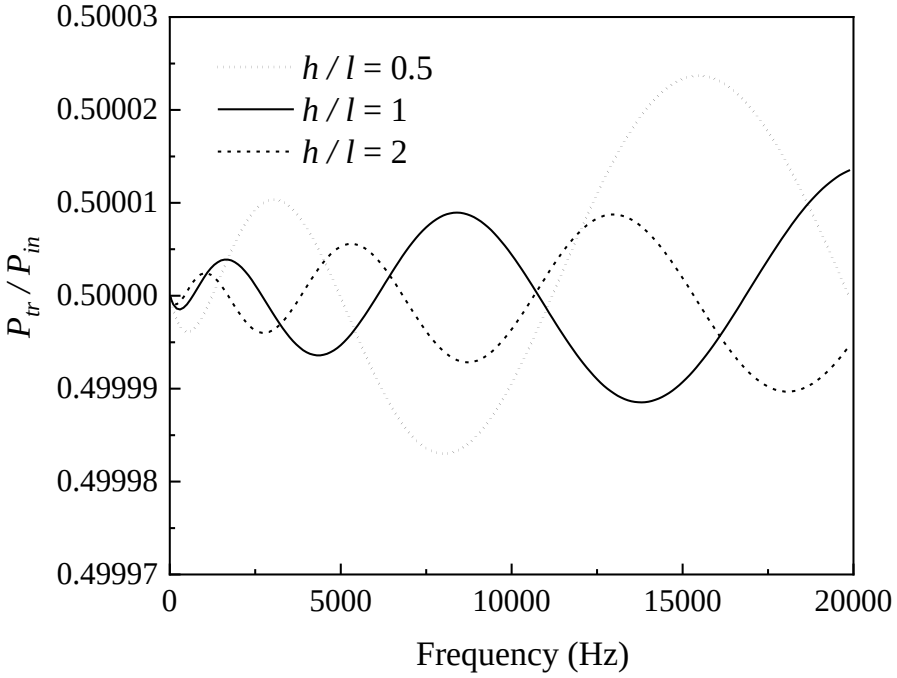

Fig. 13. Influence of h / l on the transmitted power flow versus frequency curves with L / h= 100 and a / h = 0.5.

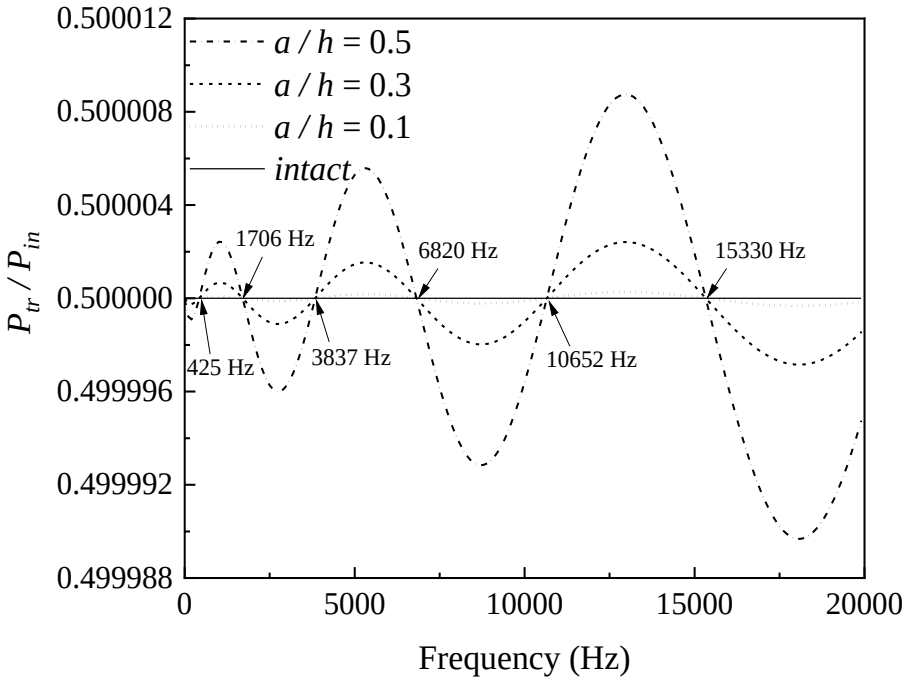

Fig. 14. Influence of a / h on the transmitted power flow versus frequency curves with L / h = 100 and h / l = 2.

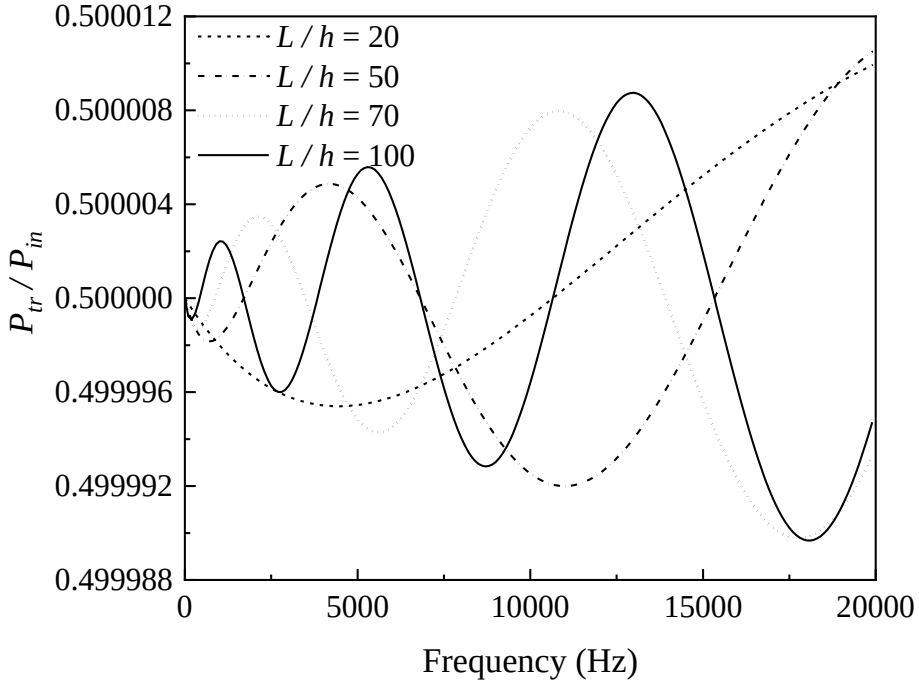

Fig. 15. Influence of L / h on the transmitted power flow versus frequency curves with $h / l = 2$ and $a / h = 0.5$.

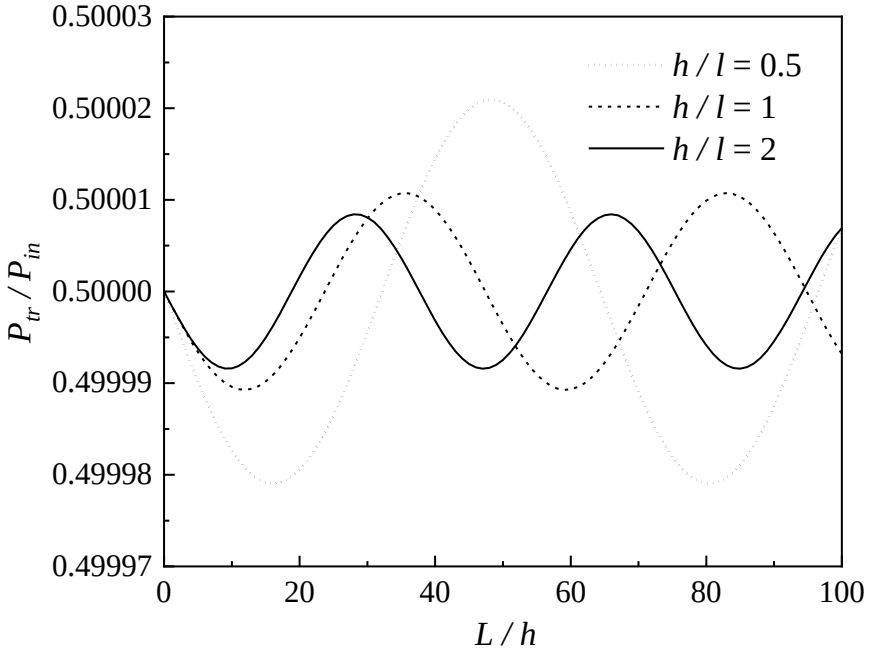

Fig. 16. Influence of h / l on the transmitted power flow versus crack location curves with f = 12000 Hz, L / h = 100 and a / h = 0.5.

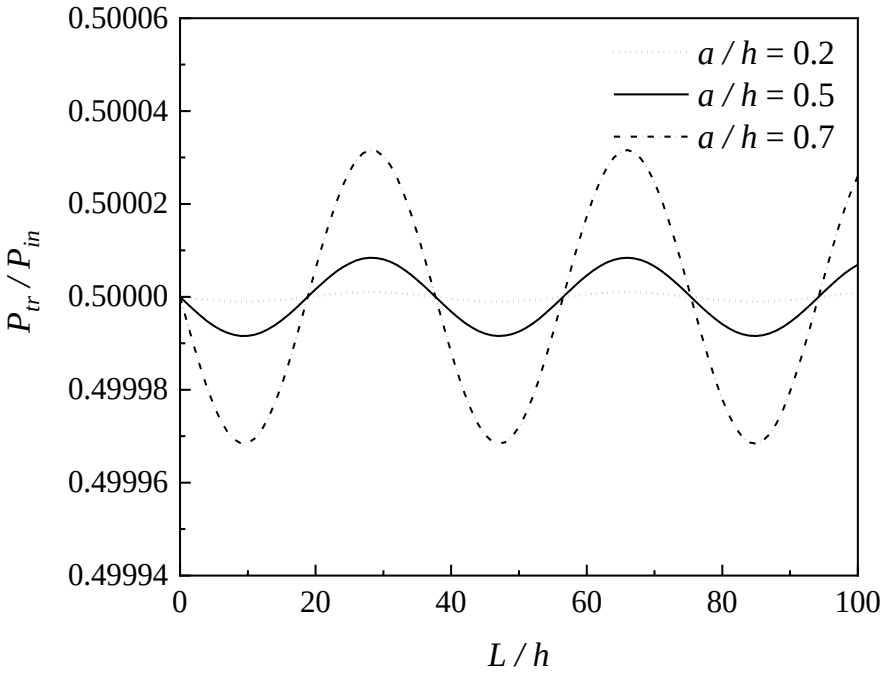

Fig. 17. Influence of a / h on the transmitted power flow versus crack location curves with $f = 12000$ Hz, $h / l = 2$ and $L / h = 100$.

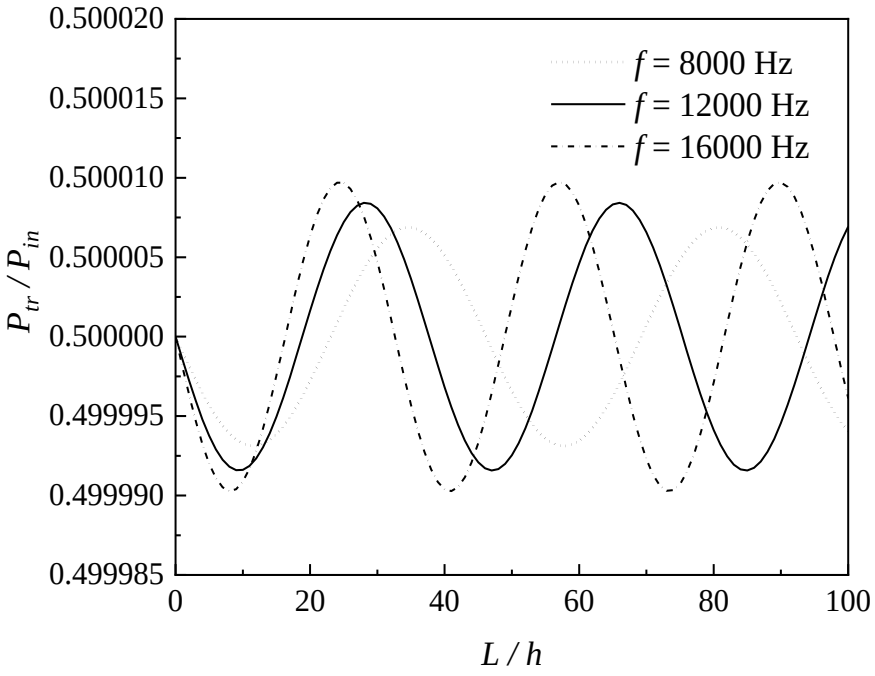

Fig. 18. Influence of f on the transmitted power flow versus crack location curves with $h / l = 2$, $L / h = 100$ and $a / h = 0.5$.